A photodegradation study of conjugated polymers for organic solar cells by absorption spectroscopy and atomic force microscopy

En studie av konjugerade polymerers fotokemiska nedbrytning genom absorptionsspektroskopi och atomkraftsmikroskopi, för tillämpning i organiska solceller

André Johansson

The Faculty of Health, Science and Technology

Master of Science in Engineering Physics

30 HP (ECTS)

Supervisors: Ellen Moons & Leif K. E. Ericsson, Karlstad University

Examiner: Lars Johansson

2021

Abstract

The effect of light exposure in ambient air on thin films made from an electron acceptor polymer poly{[N,N'-bis(2-octyldodecyl)naphthalene-1,4,5,8-bis(dicarboximide)-2,6-diyl]-alt-5,5'-(2,2'-bithiophene)} (N2200), an electron donor polymer Poly[[2,3-bis(3-octyloxyphenyl)-5,8-quinoxalinediyl]-2,5-thiophenediyl] (TQ1) and their blends, has been studied using UV-vis spectroscopy and Atomic Force Microscopy (AFM). For solutions of TQ1, N2200 and blends, the linearity of the Beer-Lambert law for absorption spectroscopy has been verified. The measured UV-vis spectra show that TQ1 thin films are more sensitive to degradation by simulated sunlight than N2200 films. They also show that among the polymer blends, the N2200-rich blend with volume ratio 1:2 (TQ1:N2200) was less sensitive to degradation by simulated sunlight than blends of ratio 1:1 and 2:1. The AFM images showed a change in roughness between the undegraded and degraded films, where the TQ1, 1:1 and 1:2 films obtained lower roughness after 45 hours of degradation, and the N2200 and the 2:1 films obtained higher roughness.

Sammanfattning

Effekten av simulerad solljusexponering i omgivande luft på tunna filmer gjorda av en elektronaccepterande polymer poly{[N,N'-bis(2-octyldodecyl)naphthalene-1,4,5,8-bis(dicarboximide)-2,6-diyl]-alt-5,5'-(2,2'-bithiophene)} (N2200), en elektrondonerande polymer Poly[[2,3-bis(3-octyloxyphenyl)-5,8-quinoxalinediyl]-2,5-thiophenediyl] (TQ1) och deras blandningar, har undersökts genom ultraviolett-synlig-spektroskopi (UV-vis-spektroskopi) och atomkraftsmikroskopi (AFM). Genom lösningar av TQ1, N2200 och blandningar, har det linjära förhållandet i Beer Lamberts lag för absorptionsspektroskopi verifierats. De mätta UV-vis-spektrumen visar att tunna TQ1-filmer är känsligare mot degradering genom simulerat solljus än tunna N2200-filmer. De visar också att den N2200-rika blandningen med ett volymförhållande av 1:2 (TQ1:N2200) var mindre känslig för degradering av simulerat solljus än blandningar med volymförhållandet 1:1 och 2:1. AFM-bilderna visade en förändring i råhet mellan degraderade och icke-degraderade filmer, där TQ1-, 1:1-, och 1:2-filmerna fick en lägre ytråhet efter 45 timmar av degradering, och N2200- och 2:1-filmera fick en högre ytråhet.

Acknowledgements

Firstly, I want to thank my supervisors Ellen Moons and Leif Ericsson for giving me the opportunity to do this project, for all the support, encouragement, and insightful discussions.

I would also like to thank Ishita Jalan for teaching me about solution and thin film preparation, and for answering all my questions during this project.

Lastly, I want to thank my family and friends for all the support during my studies.

Table of contents

1 Introduction

1.1 Background

Energy generation in the form of solar power has a great advantage over coal or oil when looking at the environmental impact. While coal and oil power plants release huge amounts of greenhouse gases into the atmosphere during energy production, solar cells are free from these types of emissions. This is beneficial to both individuals and the environment.

Due to several factors setting organic solar cells (OSCs) apart from other types of solar cells, there are specific applications and areas that these types of solar cells are highly suited for. Some of these factors are their high flexibility, light weight, low production cost, non-toxic active layers, and ability to be tuned to obtain different colours and shades. These factors make OSC fitting for several different applications where other types of solar cells are not suitable. One such application is building integration, for example integration into windows where transparent or semi-transparent OSCs can be used. Similarly, OSCs can, due to their light weight and flexibility, be integrated into different means of transportation like cars, busses, or airplanes. In transportation the weight of added solar cells is an important factor but it is also important to be able to curve and bend the solar cells along the vehicle so to not disrupt the aerodynamics. Another use of OSCs is clothing integration; by letting OSCs be integrated into wearables e.g., backpacks and jackets, they could provide the opportunity to charge devices on the go in situations where electricity is not accessible. In the case of clothing integration, the light weight, flexibility, and colour tunability of the OSCs are important factors that make these types of solar cells suitable for such applications. OSCs can also be used for portable devices like battery chargers, different types of remotes, or lamps. Furthermore, OSCs can be used as an alternative to silicon solar cells where the installation of silicon solar cells is not applicable for economical or practical reasons. Due to the low production cost, flexibility, and the light weight of OSCs, they can also easily and cheaply be transported to places where electric grids are missing, for example poor areas in developing countries. This would bring the possibility for communities, organisations, and individuals to obtain electricity for things like lighting, charging batteries, or refrigeration of medication and vaccines.

OSCs are not yet widely produced commercially but has in lab settings reached a PCE of over 18% [1] which has brought the efficiency of OSCs to the lower end of the commercially available silicon solar cells, which has an efficiency of around 18 to 22% [2]. So far single-junction crystalline silicon solar cells have achieved a PCE of over 26% [3] and perovskite solar cells have reached a PCE over 25% [3] in lab settings. But even though the PCE of OSCs is lower than silicon solar cells and perovskite solar cells, they have other advantages. They are cheaper to produce, much more flexible, and have a much lighter weight than silicon solar cells. And in opposite to perovskite solar cells, which also has a low production cost, high flexibility, and light weight, OSCs do not contain toxic heavy metals which could be harmful to the environment.

Two of the biggest obstacles for OSCs to overcome for their commercialisation is the environmental degradation of the active layer and the synthetic difficulties of manufacturing active layers since it is harder to obtain the desired active layer in a large-scale process in a factory than in a small-scale process inside a lab. The degradation mechanism and the design rules for improving their stability has to be studied to combat these issues.

Non-fullerene acceptors (NFAs) have shown great potential as the electron acceptor molecule for photo-active layers in bulk heterojunction polymer solar cells achieving a power conversion efficiency (PCE) of over 18% [1] when using small molecule acceptors and polymer donors, while full-polymer organic solar cells have reached a PCE of over 14% [4]. However, it is just in the last five years that NFAs have replaced fullerene acceptors as the most common choice in bulk heterojunction solar cell studies. Solar cells using fullerene acceptors have achieved a PCE of around 11% [5,6]. The delocalised LUMOs of the fullerene acceptors gives a high electron mobility and allows for efficient percolation. Their shape also makes them fitting for bulk heterojunctions. However, there are some disadvantages with using fullerene acceptors in the photo-active layer, such as dimerization in absence of oxygen [7,8] and photooxidation [9,10]. These fullerenes are also expensive to synthesis, have energy levels that are hard to alter and have low absorptivity in the visible region of the electromagnetic spectrum. NFAs on the other hand have a higher absorption in the visible region of the electromagnetic spectrum that can more easily be altered to fit the absorption of the donor, and they are also cheaper to synthesise. Therefore, NFAs are of great interest in the studies of polymer solar cells. In this study the electron acceptor polymer poly{[N,N'-bis(2-octyldodecyl)naphthalene-1,4,5,8-bis(dicarboximide)-2,6-diyl]-alt-5,5'-(2,2'-bithiophene)} (Polyera ActivInk N2200), or simply N2200 was studied on its own and as a blend with the electron donor polymer Poly[[2,3-bis(3-octyloxyphenyl)-5,8-quinoxalinediyl]-2,5-thiophenediyl] (TQ1). N2200 was first synthesised in 2009 [11] and so far, N2200 has achieved a PCE of over 11% when used in organic solar cells [12]. TQ1, when paired with the fullerene acceptor $PC_{70}BM$, has achieved a PCE of just over 7% [13].

1.2 Purpose

The purpose of this study was to obtain information and understanding of the photodegradation that takes place in active layers made from the polymers N2200 and TQ1 which can be used in polymer solar cells. The stability of thin films made of N2200, TQ1 and their blends of volume ratios 1:1, 1:2 and 2:1 were studied using UV-vis spectroscopy before and after undergoing degradation by exposure to simulated sunlight and ambient air. Solutions of the polymers and polymer blends were also studied by UV-vis spectroscopy to verify the agreement with the Beer-Lambert law. The surface morphology of the undegraded and degraded films were studied using an atomic force microscope in air.

2 Theory

2.1 Molecular energy levels

Conjugated polymers, like TQ1 and N2200, are polymers that contain a backbone chain with altering single- and double-bonds. The overlapping p-orbitals in the polymers creates a system of delocalised π-electrons that give these polymers interesting electrical properties and are therefore of interest in polymer solar cell studies.

HOMO, the highest occupied molecular orbital, is the highest orbital in a molecule that contain electrons and LUMO, the lowest unoccupied molecular orbital, is the lowest orbital in a molecule that do not contain electrons. The HOMO and the LUMO are the two orbitals in a molecule that are the closest to each other and therefore creates the gap across which the electronic excitation occurs.

In the case of organic photovoltaics, two polymers are usually used, where one polymer acts as the electron donor, and one acts as the electron acceptor. These polymers are mixed to create a bulk heterojunction (BHJ), depicted in figure 1. This BHJ is kept between a cathode and an anode. The donor has a higher HOMO and LUMO than the acceptor as shown in figure 2.

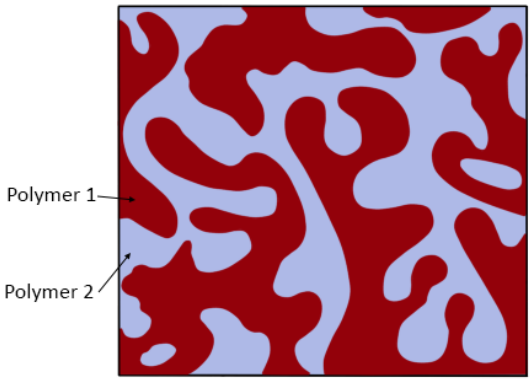

Figure 1. *Bulk heterojunction made from two polymers.*

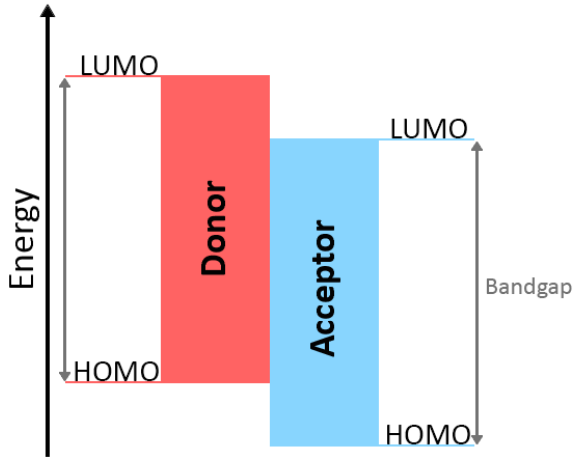

Figure 2. *Energy diagram of a donor-acceptor bilayer, showing HOMO and LUMO levels.*

An organic semiconductor can absorb incoming photons. If the incoming photon energy is equal to the HOMO-LUMO gap, an electron will be excited from the HOMO to the LUMO. If the incoming photon energy is greater than the HOMO-LUMO gap, the electron may jump to a higher energy level than the LUMO, one of several vibrational states, and then decay down to the LUMO in a process called thermalisation (loss of energy through heat loss).

In the active layer of the solar cell, consisting of two polymers, the excited electron in the donor material gets transferred from the LUMO of the donor to the LUMO of the acceptor, while the hole stays in the HOMO of the donor. Since the two carriers are still attracted to each other, they form a charge-transfer state. While in this state, there is still potential for the carriers to recombine, but when the thermal energy overcomes the binding energy between the hole and the electron, the charges are separated. The carriers are then free to move to either the cathode, in case of electrons, or the anode, in case of holes. A simplification of this process is shown in figure 3.

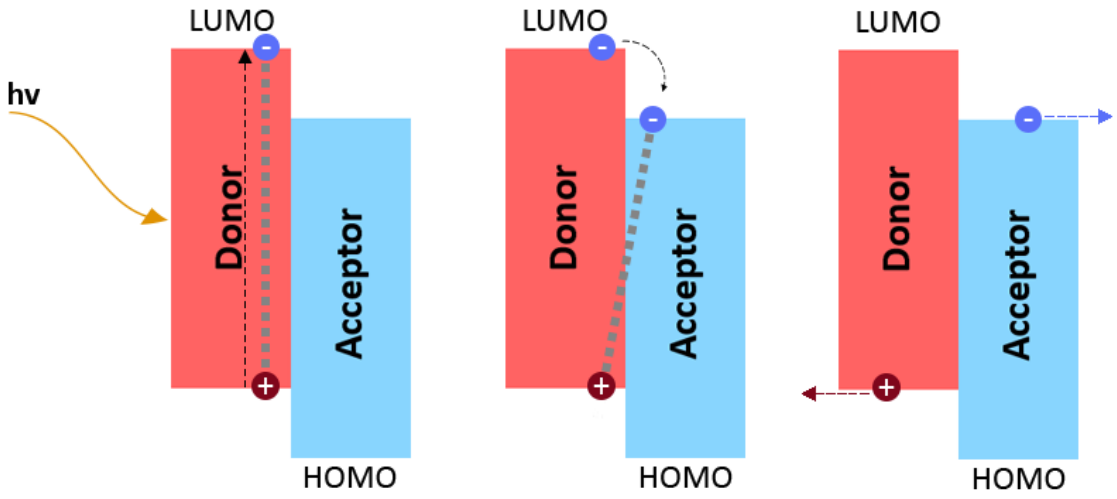

Figure 3. *Process of photon absorption and charge generation in an active layer of an organic solar cell made from an electron donor and an electron acceptor.*

The molecular weight of a polymer can be described in several different ways, the most common are number average molecular weight (Mn) and weight average molecular weight (Mw). Mn is obtained by dividing the total weight of all the polymer chains by the total number of polymer chains. While Mw, as opposed to Mn, takes the molecular weight of the chains into consideration when determining the contributions to the weight average. A bigger chain contributes more to Mw. The fraction of these weights (Mw divided by Mn) is called polydispersity index (PDI) and describes the width of the distribution of molecular weights. The definitions of Mn and Mw is shown in equations (1) and (2). The larger the width, the broader is the distribution. A PDI of 1.0 would mean that all the chains in the sample have the same length and thus have the same molecular weight. Mn and Mw are measured by using size-exclusion chromatography (SEC) [14, 15, 16].

$$M_n = \frac{\sum N_i M_i}{\sum N_i} \quad (1)$$

$$M_w = \frac{\sum N_i {M_i}^2}{\sum N_i M_i} \quad (2)$$

$M_i = \ molecular\ weight\ of\ one\ chain$
$N_i = \ number\ of\ chains\ of\ that\ molecular\ weight$

2.2 Ultraviolet-visible spectroscopy

Ultraviolet-visible spectroscopy is used to obtain an absorption, reflectance, or transmittance spectrum of a species in the full visible range and parts of the UV-range of the electromagnetic spectrum. The species being studied can be in several different forms, such as solution, thin film, or powder. In a UV-vis spectrophotometer, the light is passing through the sample and a detector on the other side measures the percentage of transmitted light. When measuring, the solvent and cuvette, in case of studying a solution (fig. 4 a), or the substrate, in case of studying thin films (fig. 4 b), will themselves absorb and reflect some of the incoming radiation and give a background absorption or transmittance spectra. To prevent this, a baseline measurement is performed by measuring the transmittance of the light passing through either a cuvette containing pure solvent, in the case of solution measurements, or a clean substrate, in the case of thin film measurements. By doing so the radiation absorbed or reflected by the solvent, cuvette, and substrate can be omitted and a spectrum for only the compound can be obtained.

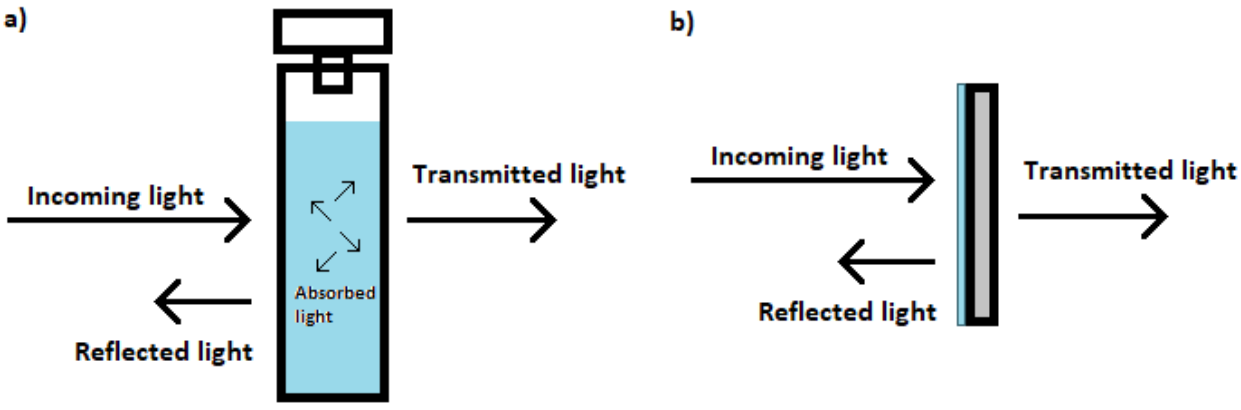

Figure 4. *Absorption, reflectance, and transmittance of incoming light in UV-vis spectroscopy for solution in cuvette (a) and thin film on substrate (b).*

The UV-vis spectrophotometer uses double beams, where one beam goes through the sample and one beam, the reference beam, goes through the air directly into a detector. By doing this the reference beam can compensate for fluctuations from the source and these fluctuations can be cancelled out, giving a more accurate measurement. The measurements on solutions in this project were made using a cuvette sample holder (fig. 5). The thin film measurements were made using a diffuse reflectance accessory (DRA) (fig. 6). A DRA uses an integrating sphere to capture the transmitted or reflected electromagnetic radiation simultaneously. The inside of the sphere is highly reflective and incoming radiation will undergo many diffuse reflections. In transmittance mode, the thin film is placed at the transmittance port, shown in figure 6, and the incoming radiation, going through the sample, can then dissipate in three ways. The largest part of incoming light will eventually be absorbed into the sphere walls, a small portion will go out through the empty ports, and the rest will go into the detector inside the sphere. Since the radiance along the inside surface of the sphere is uniform and proportional to the source input flux, the sphere detector has the ability to sample the radiance of the inside surface and then relay the detector signal for processing, and in that way obtain a correct measurement [17,18]. When using double beams with an integrating sphere, the beams are temporally sequenced by the chopper of the instrument, meaning that only one beam is present in the sphere at any given time. This is an important step to ensure that the spectrophotometer can distinguish between the reference beam and the sample beam and give a correct measurement [17,18].

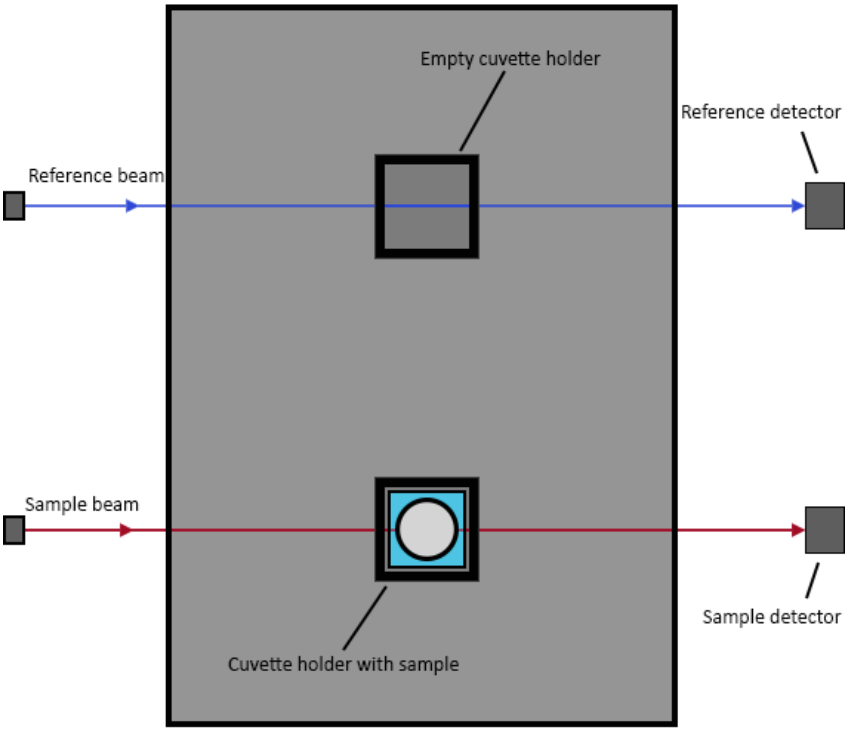

Figure 5. *Cuvette holder for solution measurements (top down view). The figure shows the sample beam (red) pass thourgh the cuvette holder holding a cuvette containing the solution, and the reference beam (blue) passing through the empty cuvette holder. The sample beam continues into the sample detector and the reference beam continues into the reference detector.*

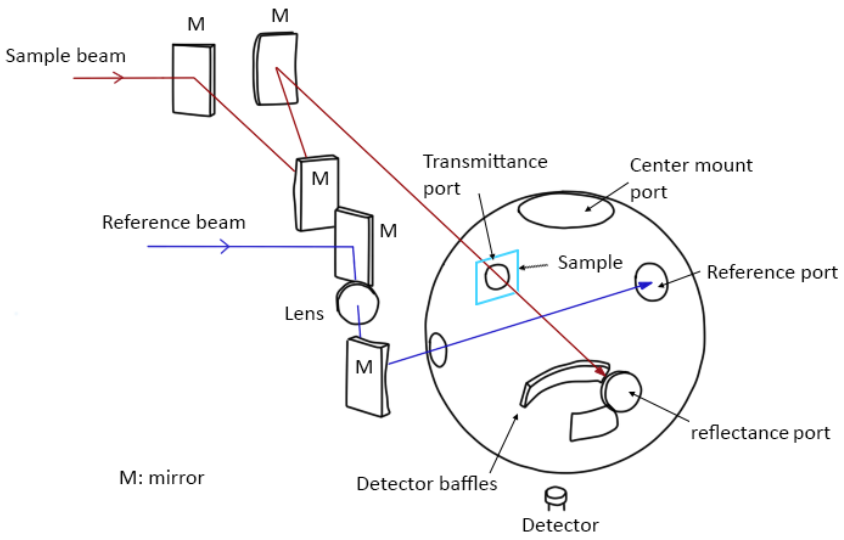

Figure 6. *Integrating sphere used in a diffuse reflectance accessory for UV-vis spectroscopy. The figure shows the incoming sample beam (red) being reflected by three mirrors and enter the sphere through the transmittance port. The incoming reference beam (blue) is reflected by two mirrors and passes through a lens and enters through one of the reference ports.*

The spectrophotometer always measures transmittance when obtaining an absorption spectrum, the computer program used translates the transmittance to absorbance using the formula shown in equation (3) [19].

$$A = 2 - log_{10}(T) \qquad (3)$$

Where A is the absorbance and T is the transmittance given in percent.

Equation (3) is obtained though the Beer-Lambert law. The law relates the transmitted intensity I_t to the concentration c, the sample path length l, the molar attenuation coefficient ε_λ, and the incoming intensity I_0, at each wavelength λ as:

$$I_t = I_0 \cdot 10^{-\varepsilon_\lambda \cdot c \cdot l}$$

And can be rewritten as:

$$log_{10}\left(\frac{I_t}{I_0}\right) = -\varepsilon_\lambda \cdot c \cdot l = -A$$

$$-log_{10}(T') = A$$

$$-log_{10}\left(\frac{T}{100}\right) = log_{10}(100) - log_{10}(T) = 2 - log_{10}(T) = A$$

$$A = 2 - log_{10}(T)$$

Where A is the absorbance, T' is the transmittance in decimal form, and T is the transmittance in percent.

2.3 Absorption spectra

In quantum mechanics, molecular orbitals can be expressed as a linear combination of atomic orbitals where the electron configurations of the atoms are described as wavefunctions. When two atoms are brought close together their orbitals can either undergo constructive or destructive interference. Constructive interference between two orbitals will reinforce their intensity and create a bonding orbital, and destructive interference between two orbitals will decrease their intensity and create an anti-bonding orbital. The bonding orbital is lower in energy than the anti-bonding orbital and will therefore fill up with electrons first. Because of this, a molecule usually has many more energy levels than an atom and as a result the absorbed light creates a broader absorption peak than that of atoms. The absorption of a photon leads to the transition of an electron from a lower energy level to a higher energy level. The species absorbs the energy in form of visible and ultraviolet light that excites the electrons in bonding or non-bonding orbitals of the molecules to higher anti-bonding molecular orbitals. Four different types of transitions can take place: π–π^*, n–π^*, σ–σ^*, and n–σ^*, where π^* and σ^* stands for anti-pi bond and anti-sigma bond, respectively. The HOMO-LUMO gap is the onset of absorption. The absorbance of a polyatomic molecule is a result of not only the change in electronic state but also the vibrational and rotational states of the molecule. The energy that is absorbed by a molecule can be divided into three components, the electronic energy, the vibrational energy, and the rotational energy. The electronic energy is the energy of the molecule that comes from the different energy states of the molecule's bonding electrons. The vibrational energy is related to several different interatomic vibrations that take place inside the molecule, and the rotational energy is the energy that comes from several different rotational motions occurring in the molecule. The distance between electronic energy levels is larger than the distance between the vibrational energy levels, as shown in the Jablonski diagram in figure 7. Similarly, the distance between the rotational energy levels is smaller than the distance between the vibrational energy levels. This means that the vibrational energy levels are superimposed upon the electronic energy levels and in turn the rotational energy levels are superimposed upon the vibrational energy levels. The absorption of energy within the visible or ultraviolet part of the electromagnetic spectrum results in an electronic transition of an electron from the ground state to an excited state. If the absorbed energy lies within the infrared part of the electromagnetic spectrum, the transition occurs between two vibrational states.

The electrons in a single molecule at 0 K have discrete electronic energy levels and the absorption of a photon would therefore generate the transition of an electron between these discrete energy levels, resulting in a discrete absorption peak. At higher temperatures, the molecule begins to vibrate and rotate which makes it possible for several different electron transitions between the ground electronic level and several vibrational levels of higher electronic levels to take place [20].

The shape of the absorption peaks is determined by several different factors within the polymer, e.g., the molecular weight, the PDI, and the polymer conjugation length. The conjugation length describes how delocalised the electron cloud is for an electron with a certain energy, e.g., an electron in the HOMO is delocalised in a certain part of the polymer chain with a certain length, this length being the conjugation length. Similarly, when the electron gets excited to the LUMO the electron will have a certain delocalisation there as well.

Where the peak maxima of an absorption spectrum lie are given by the energy difference between the HOMO and the LUMO, i.e., the HOMO-LUMO gap or bandgap. The energy of the electronic transition due to excitation by a photon is inversely proportional to the wavelength of the photon, as shown in equation (4), e.g., a transition with an energy of 2.0 eV will give an absorbance maximum at roughly 620 nm. The HOMO-LUMO gap can be influenced by the length of the polymer chain, the number of monomers a chain contains, and the conjugation length. [21, 22].

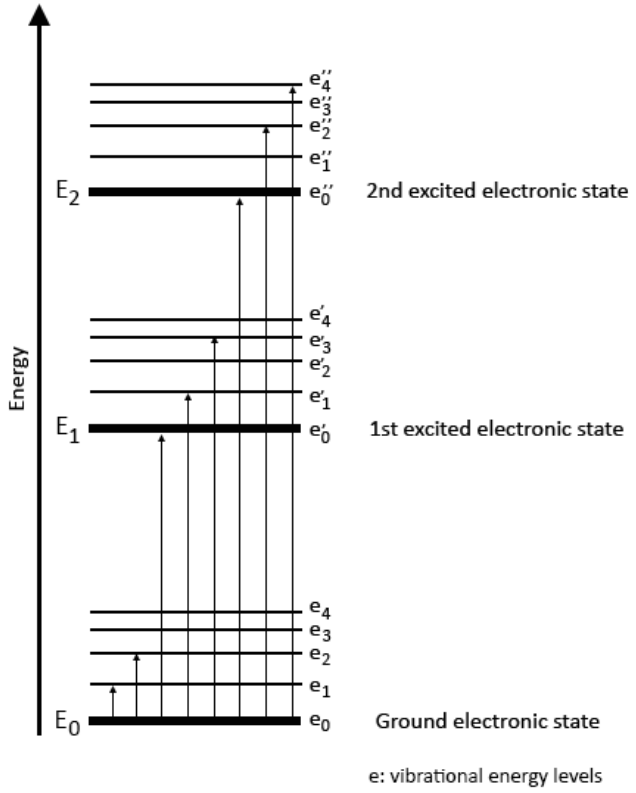

Figure 7. *Jablonski diagram showing electronic and vibrational energy levels and absorption lines.*

$$\lambda = \frac{h \cdot c}{E} \qquad (4)$$

E = photon energy, c = speed of light in vacuum,

h = Planck constant, λ = wavelength of photon

Oligomers consisting of just a few monomers can have a significantly different spectrum than longer polymers. This is because the length over which the electrons can be delocalised is longer than the length of the molecule, in the case of monomers or short oligomers. Confining the electrons to a shorter chain will widen its bandgap due to quantum confinement effects. As the chain length increases, the HOMO-LUMO gap reduces. This has been shown in previous work where the gap went from roughly 3.8 eV for the single TQ1 monomer to 2.48 eV for the TQ1 oligomer consisting of eight monomers [21]. The conjugation length can also be limited due to disorder and kinks appearing in the polymer chain. This is because disorders and kinks can break the conjugated length and shorten the length of the electron delocalisation [21]. The effect of increasing number of monomers is limited

to the effective conjugation length where adding more monomers will not have any further effect and the bandgap will saturate to a certain value for all polymers longer than this length. As an example, this number is around 9 monomers in the case of TQ1 [21].

A monomer of TQ1 has a weight of 619 g/mol and a monomer of N2200 has a weight of 990 g/mol. Dividing the Mn of the polymer by the weight of the monomer gives an average of the number of monomers in the polymer. For the polymers used in this study, the molecular weights, Mn, are 44000 g/mol for TQ1 and 54000 g/mol for N2200. This gives TQ1 an average length of around 79 monomers, and N2200 an average length of about 126 monomers. But since the TQ1 and N2200 used in this study have a PDI of 3 and 2.3, respectively, there will be a big variation among the polymer chain length. In any case, the length of the polymer chains used in this study can be considered considerably longer than the effective conjugation length.

The temperature of the solution containing the polymer can also affect the position of the absorption peak maxima and the width, as shown in earlier studies [22]. The surrounding of the polymers also plays a part in the positions and the shape of the absorption maxima since the polymers can interact with their surroundings. Intermolecular interactions can take place between the polymers in both solution and film; however, molecules are much denser packed in a solid film than in a dilute solution, hence the intermolecular interaction between the molecules is expected to be more significant in a film. This usually leads to a strong shift in the absorption peaks in the film spectrum compared to the corresponding solution spectrum. In the case of solutions, the polymers may even interact with the solvent making different transitions possible.

2.4 Beer-Lambert Law

The Beer-Lambert law states that one can relate the absorbance of a material containing a single attenuating species of uniform concentration to the optical path length through the sample, the optical attenuation of the species, and the concentration of the species. The formula expressing this is given in equation (5).

$$A = \varepsilon_\lambda \cdot l \cdot c \tag{5}$$

Where A is the absorbance, ε_λ is the molar attenuation coefficient of the attenuating species, l is the optical path length and c is the concentration of the attenuating species [23].

The Beer-Lambert law can also be used for blends where two different attenuating species are used, provided that the species do not interact. The formula for blends is shown in equation (6).

$$A = \varepsilon_1 \cdot l \cdot c_1 + \varepsilon_2 \cdot l \cdot c_2 \tag{6}$$

Where ε_1 and ε_2 are the molar attenuation coefficient for the two different species and c_1 and c_2 are the total concentration of the respective species in the solution.

2.5 Vibrational spectra

The types of vibrations a molecule may undergo are divided into two categories: bending and stretching vibrations. Bending vibrations change the angle between two bonds while stretching vibrations changes the interatomic distance between two atoms along the same axis [20]. Vibrational stretching is divided into symmetric and asymmetric stretching as seen in figure 8 a) and b), and bending stretching is divided into four categories: twisting, scissoring, wagging, and rocking as shown in figure 9 a) to d).

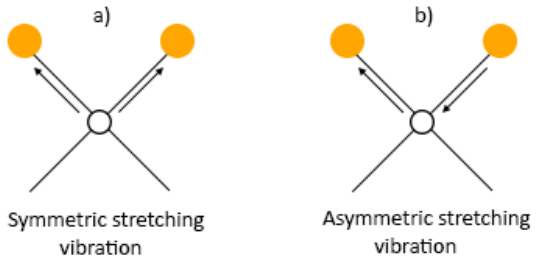

Figure 8. *Symmetric and asymmetric stretching vibration.*

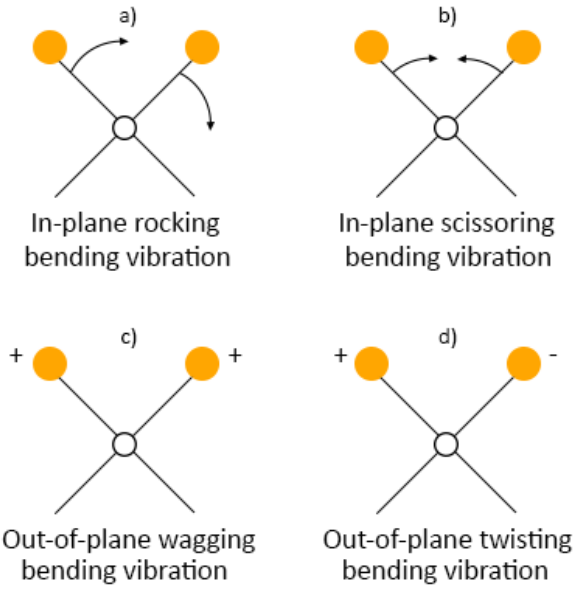

Figure 9. *Different types of bending vibrations. "+" indicates motion out of the page, "-" indicates motion into the page.*

2.5 Atomic force microscopy

In an atomic force microscope (AFM), images of a material's surface morphology can be obtained by measuring atomic forces. The surface of a sample is scanned in a raster pattern by a tip attached to a force-sensing and flexible cantilever. The sample rests on a piezoelectric tube scanner that moves the sample under the tip during the scanning process. These movements are induced by applying

voltage, making the piezo either contract or expand in different ways. A laser is pointed at the end of the cantilever and reflected onto a position-sensitive deflector. The laser is part of a feedback loop where the position of the laser will give the system information about the cantilevers position and oscillation. The basic set up of the AFM is shown in figure 10. An AFM can be driven in three different modes: Contact mode, non-contact mode and tapping mode. In this study, tapping mode was used. In tapping mode, the cantilever is made to oscillate at or near its resonance frequency, this is usually done by a piezo element that is positioned at the base of the cantilever. While scanning in tapping mode the amplitude of the driving signal and the frequency is kept constant. As the cantilever oscillates and the tip comes close to the surface the cantilever experience forces that lead to a change in the amplitude of the oscillations. These changes in amplitude are used as feedback and the height is managed such that the oscillation amplitude is kept at the constant set value. The change of the cantilever height is then used to create the height image of the sample [20].

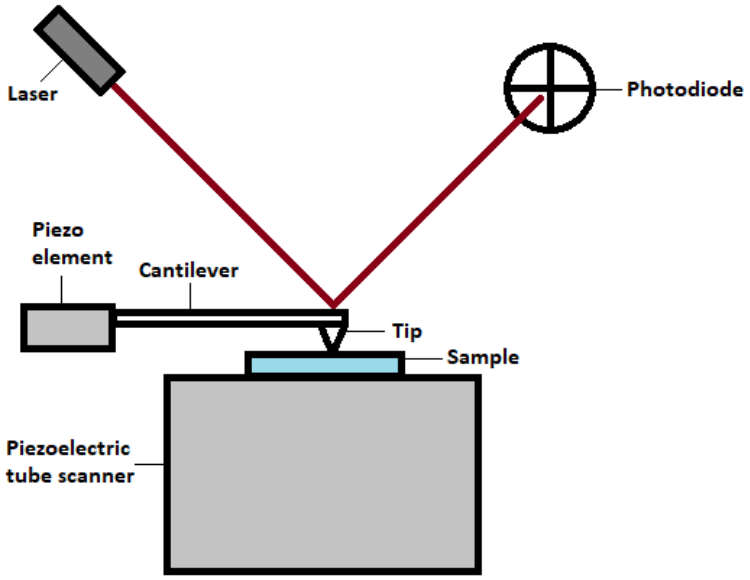

Figure 10. *Basic setup of an atomic force microscope*

3 Experimental section

3.1 Materials

The TQ1 used in this study was synthesized by Dr Desta Gedefaw at Chalmers university and had a weight average molecular weight (Mw) and a number average molecular weight (Mn) of 133 kg/mol and 44 kg/mol, respectively. The N2200 used was purchased from Ossila (Great Britain) and had a Mw and Mn of 125 kg/mol and 54 kg/mol, respectively. The molecular structures of TQ1 and N2200 are shown in figure 11 a) and b). The quartz glass substrates used were 2 mm thick squares with 25.4 mm sides and was purchased from SPI Supplies (USA). The Chloroform (analysis grade) was purchased from Merck KGaA (Germany). The isopropanol (technical grade) was purchased from VWR Chemicals BDH (France).

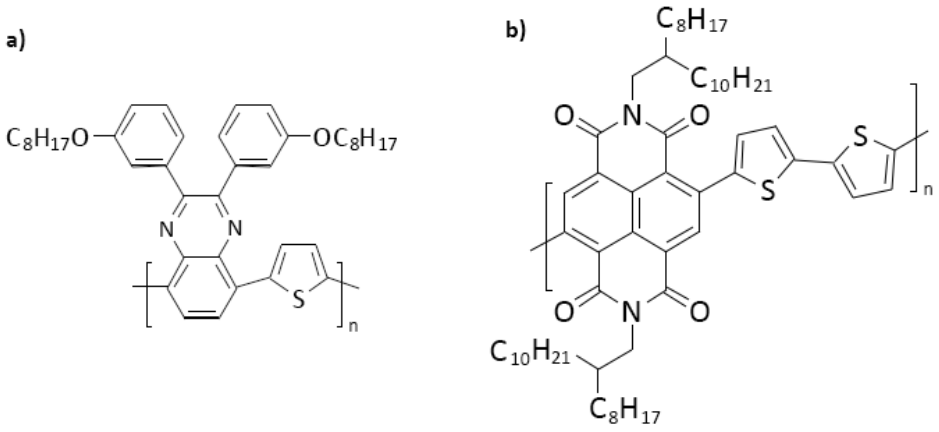

Figure 11. *Molecular structure of a) TQ1 and b) N2200*

3.2 Sample preparation

3.2.1 Thin films

The quartz glass substrates were cleaned in isopropanol using an ultrasonic bath for 60 minutes followed by ozone cleaning for 20 minutes. When being reused the substrates were cleaned with chloroform as a first step. TQ1 and N2200 solutions with a concentration of 10 g/l were prepared in amber glass vials, containing a stirrer bar, by mixing the pure polymer with chloroform. The solutions were stored on a magnetic stirrer heat plate at 190 rpm and 45 degrees Celsius overnight inside a glovebox. Polymer blends of different volume ratios (1:1, 1:2, 2:1) were mixed from the pure solutions inside the glovebox under yellow light and was left on the same heat plate overnight. The pure solutions and blends were spin coated onto quartz substrates to create thin films using a spin-coater inside the glovebox. The spin coating was done by ramping up to 100 rpm for 3 seconds, followed by going from 100 to 3000 rpm for four seconds and lastly keeping 3000 rpm for 80 seconds. The thin films underwent degradation by being exposed to ambient air and simulated sunlight (AM 1.5) using a solar simulator with an intensity of 1000W/m^2 that was calibrated using a silicon photodiode reference cell. The thin films were kept inside the glovebox when not being measured or undergoing degradation.

3.2.2 Solutions

The diluted solutions where prepared by a two-step process. First, 1980 µl of chloroform and 20 µl of the undiluted 10 g/l solution were added to an empty vial. Then, 600 µl of the newly diluted solution were mixed with 2400 µl of chloroform to obtain a diluted solution with the concentration of 0.02 g/l. The calculations for this process can be seen in equations (7) to (11).

$$c_i V_i = c_k V_k \quad (7)$$

$$10\ \mu g/\mu l \cdot 20\ \mu l = c_2 \cdot 2000\ \mu l \quad (8)$$

$$c_2 = 0.1\ \mu g/\mu l \quad (9)$$

$$0.1\ \mu g/\mu l \cdot 600\ \mu l = c_3 \cdot 3000\ \mu l \quad (10)$$

$$c_3 = 0.02\ \mu g/\mu l = 0.02\ g/l \quad (11)$$

c_i = concentration before dilution c_k = concentration after dilution

V_i = volume before dilution V_k = volume after dilution

A concentration of 0.02 g/l was chosen after some testing since the absorbance value of that concentration was between 0 and 1 a.u. when being measured by UV-vis spectroscopy.

3.3 Instruments

The UV-vis spectrometer used was a Cary 5000 UV-Vis-NIR spectrophotometer from Agilent Technologies (USA) and the software was Cary WinUV 6.1. For thin film measurements a diffuse reflectance accessory (DRA) was also used.

The solar simulator used was a Sol2A model 94022A and the silicon photodiode reference cell used was of model 91150V, both from Oriel Instruments (USA).

The atomic force microscope was a Veeco DI Innova Atomic Force Microscope from Bruker (USA) and the tip used was from Olympus (Japan) with a resonance frequency of 300 Hz. The software used was Nanoscope 9.2. For AFM image analysis the software used was SPIP and Gwyddion.

3.4 Sample characterisation

3.4.1 Thin films

The absorption spectra of the unexposed thin films of the polymers and polymer blends spin coated on quartz substrates were measured in a wavelength range of 300 to 850 nm and with a 1 nm step size using a UV-vis spectrometer with the diffuse reflection accessory (DRA). The spectra of the films were measured again after degradation by simulated sunlight and ambient air. This was repeated with degradation times of 2, 5, 10, 20, 30 and 45 hours. A clear quartz glass substrate was used as a baseline reference when measuring the absorbance. A control sample of TQ1 and N2200 thin films was also prepared and measured before and after 47 hours of degradation, to check for reproducibility of the results.

3.4.2 Solutions

Pure polymer solutions and blend solutions were diluted in two steps to a concentration of 0.02 g/l using chloroform and put into glass cuvettes. The solutions were measured in a wavelength range of 300 to 900 nm and with a 1 nm step size using a UV-vis spectrometer using a cuvette sample holder. A baseline absorption spectrum was measured using a cuvette with pure chloroform and then the absorption spectra for pure solution and blends were measured.

3.4.3 Atomic force microscopy

Height images of the films' surface were obtained using an AFM before and after 45 hours of degradation. The images were measured with a resolution of 512 lines per image with a 2 x 2 micrometre scan area and with a scan rate of under 0.5 Hz. Since the piezoelectric tube scanner surface is magnetic, a small circular metal plate was attached using double sided adhesive tabs under every film to ensure that the film stayed in place during the scanning process.

4 Results

4.1 UV-vis absorption spectra

4.1.1 Thin films

The UV-vis absorption spectra obtained from TQ1, N2200 and blend films during different stages of degradation are shown in figure 12 and 13.

The spectrum of the non-degraded TQ1 film in figure 12 a) shows two characteristic bands, one with maximum at 622 nm and one with maximum at 360 nm. These bands have been reported in previous works [24, 25]. The peak at 360 nm is a result of the π–π* electron transition in the conjugated backbone meaning that electrons of a pi bond get excited to an anti-pi bond. The peak at 622 nm is the result of a transition between HOMO and LUMO (the lowest energy transition), and has a strong intramolecular charge transfer (ICT) character, because a large fraction of an electronic charge is transferred to one region of the molecule to another (donor moiety to acceptor moiety) [26]. A gradual decrease of absorbance with increasing exposure time to simulated sunlight in air was observed, with a total decrease of the 622 nm peak by 32% after 45 hours of exposure. The peak also underwent a blueshift to 600 nm after 45 hours of degradation.

The spectrum of non-degraded N2200 in figure 12 b) shows two absorption bands, one at 390 nm and one at 700 nm. These bands are a result of a π–π* electron transition and the HOMO-LUMO transition with strong ICT character, respectively [27]. A gradual decrease of absorbance with increasing

exposure time to light in air was observed. After 45 hours of degradation the intensity of the peak at 700 nm decreased by 12% and the peak underwent a blueshift to 695 nm.

In figure 13 a) the absorption spectra of the TQ1:N2200 1:1 blend film is shown. The two absorption bands of the non-degraded blend film are located at 370 nm and 635 nm. After 45 hours of photodegradation the intensity of the 635 nm peak decreased by 34%.

Figure 13 b) shows the absorption spectra of the TQ1:N2200 1:2 film. The peaks are located at 377 nm and 641 nm. After 45 hours of degradation the peak at 641 nm decreased in intensity by 27.5%.

The absorption spectra of the TQ1:N2200 2:1 film is shown in figure 13 c) and has its peaks at 367 nm and 632 nm. The intensity of the peak located at 632 nm decreased by 40% after 45 hours of degradation.

Figure 14 shows the change in normalized absorbance with respect to the degradation time. From the figure it can be determined that TQ1 photodegrades faster than N2200. It can also be determined that the TQ1:N2200 film with a 1:2 volume ratio was the most stable to photodegradation among the blend films.

Figure 15 shows the change in normalized absorbance with respect to the degradation time for the high energy peaks. The high energy peaks follow the same pattern of degradation as the normalised degradation of the low energy peaks. For the high energy peak, N2200 had the lowest total degradation after 45 hours at 7%, the 1:2 blend had the second lowest at 12%, TQ1 had the third lowest at 17%, 1:1 had the fourth lowest at 17.5% and 2:1 had the highest degradation at 24%. The TQ1 high energy peak underwent a slight blueshift from 361 nm to 357 nm. The N2200 peak underwent a small blueshift from 393 nm to 390 nm. The 1:1 blend peak did not shift position and remained at 370 nm. The 1:2 blend peak underwent a redshift from 377 nm to 382 nm and the 2:1 blend peak underwent a slight blueshift from 367 nm to 364 nm.

A second set of TQ1 and N2200 films was made, and its absorption spectra was measured before and after 47 hours of photodegradation. The absorption spectra are shown in figure 16.

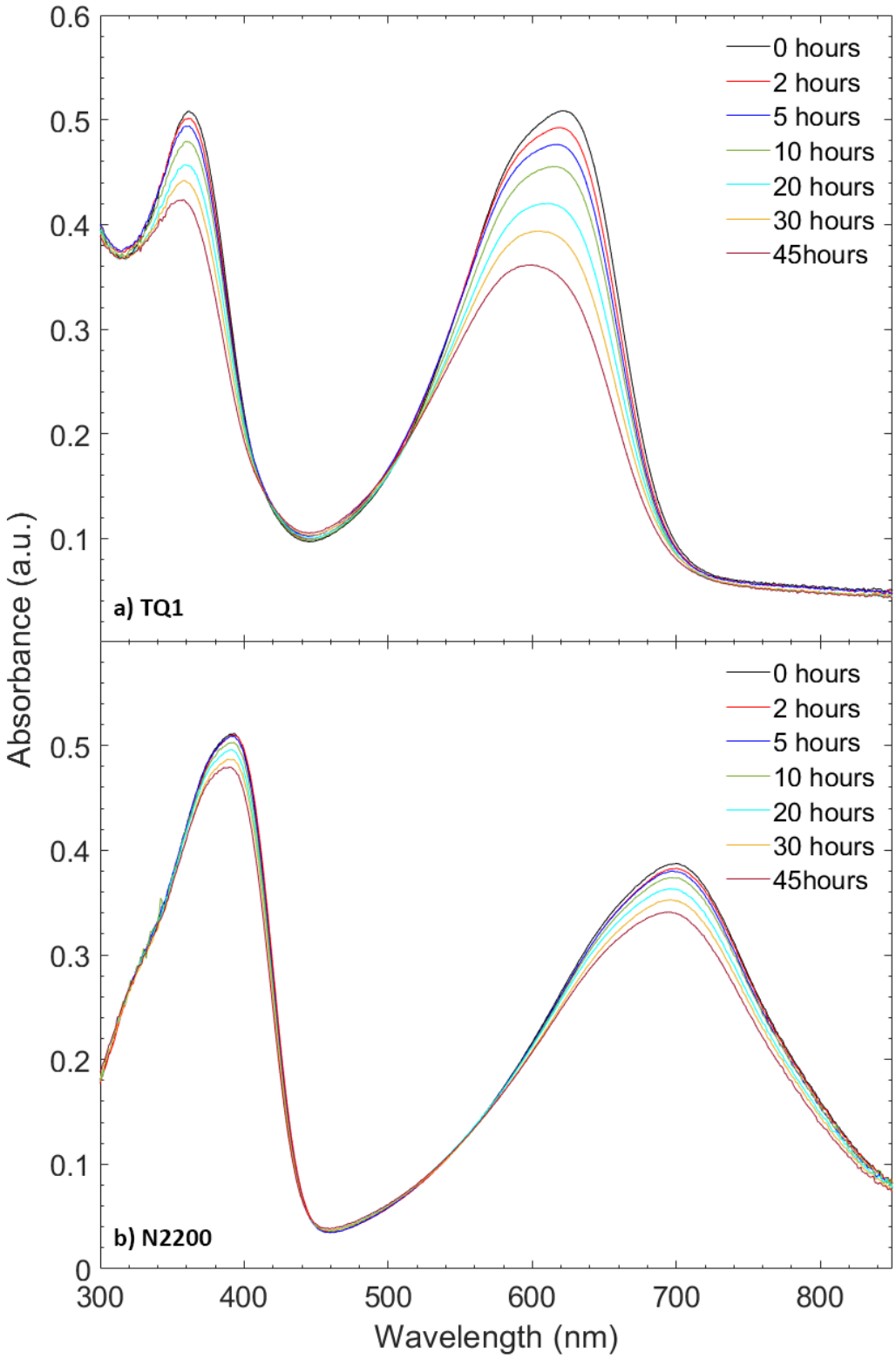

Figure 12. *UV-vis absorption spectra of a) TQ1 thin film and b) N2200 thin film for different times of photodegradation in ambient air.*

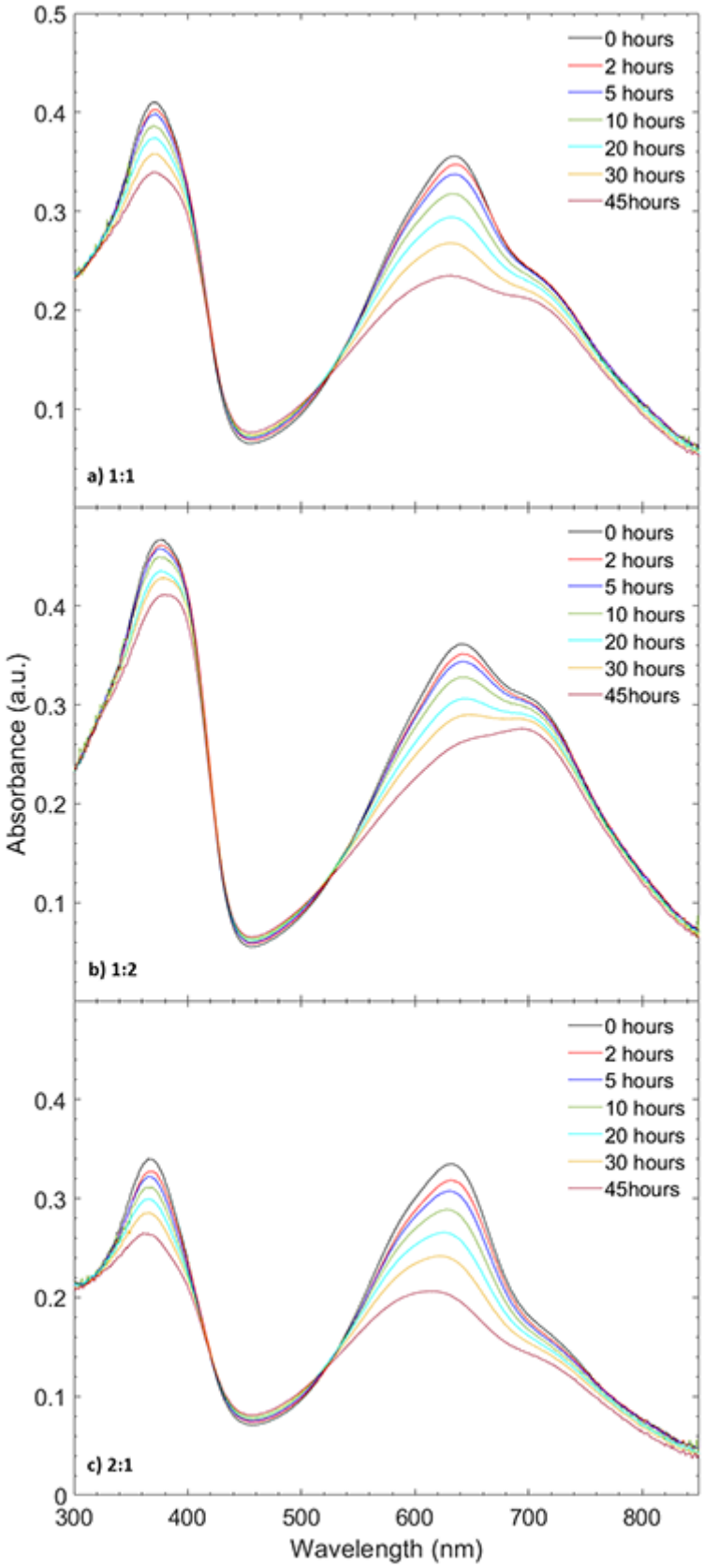

Figure 13. *UV-vis absorption spectra of polymer blend thin films of ratio a) 1:1, b) 1:2 and c) 2:1 for different times of degradation.*

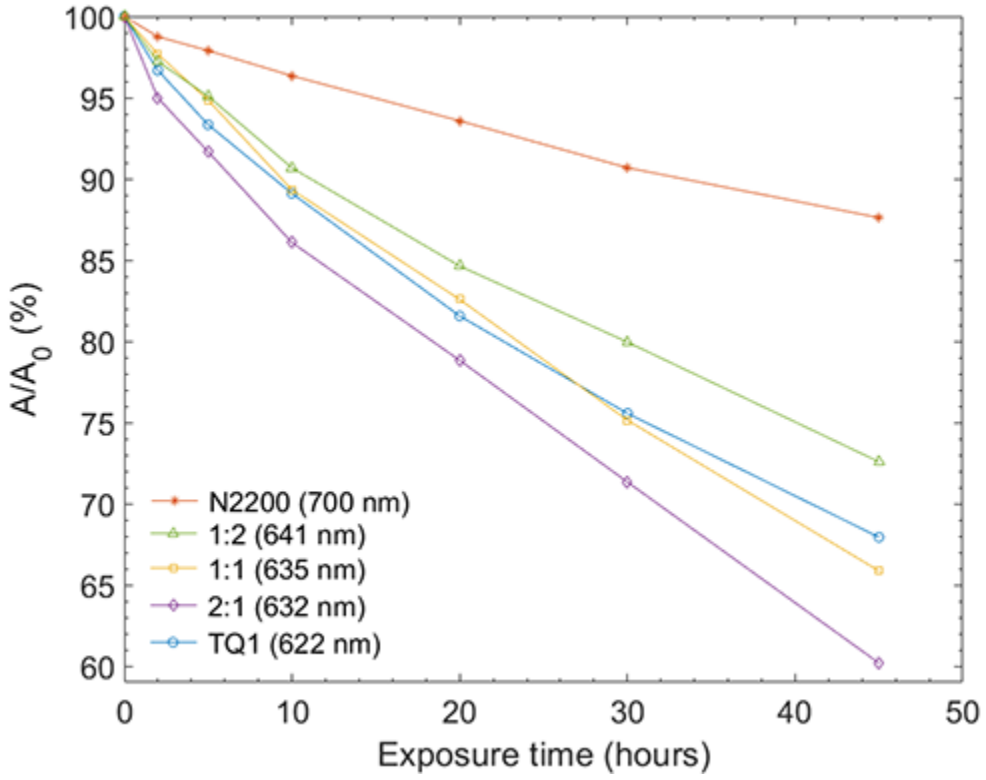

Figure 14. *Change of normalised absorbance as a function of exposure time for TQ1, N2200 and blend films for low energy peaks.*

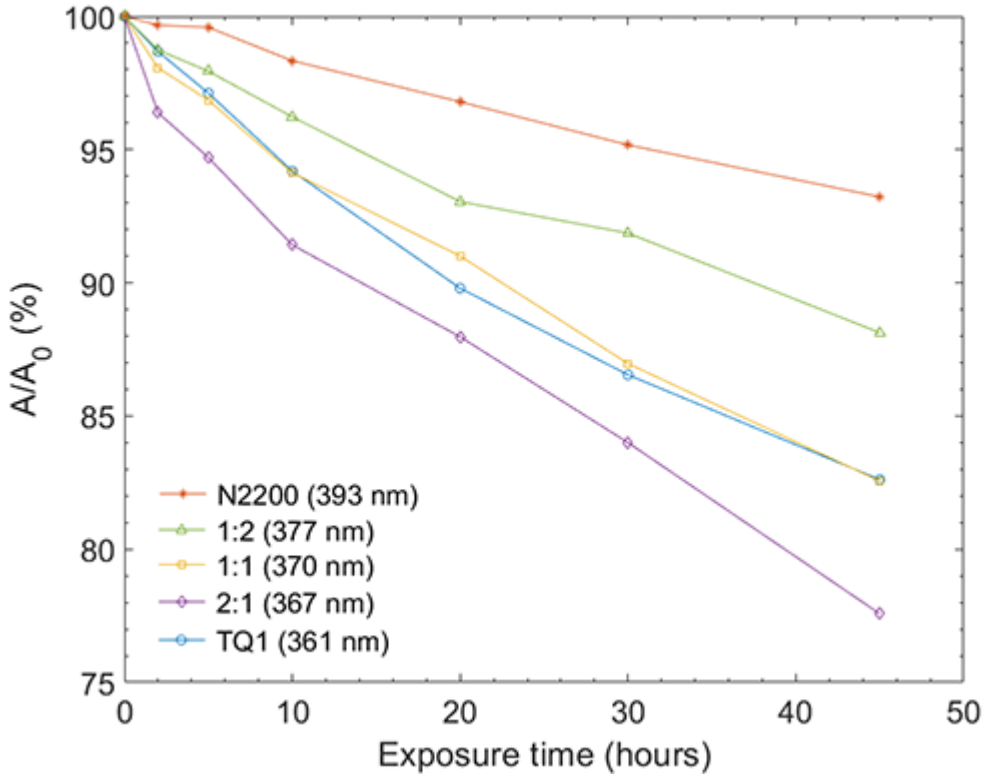

Figure 15. *Change of normalised absorbance as a function of exposure time for TQ1, N2200 and blend films for high energy peaks.*

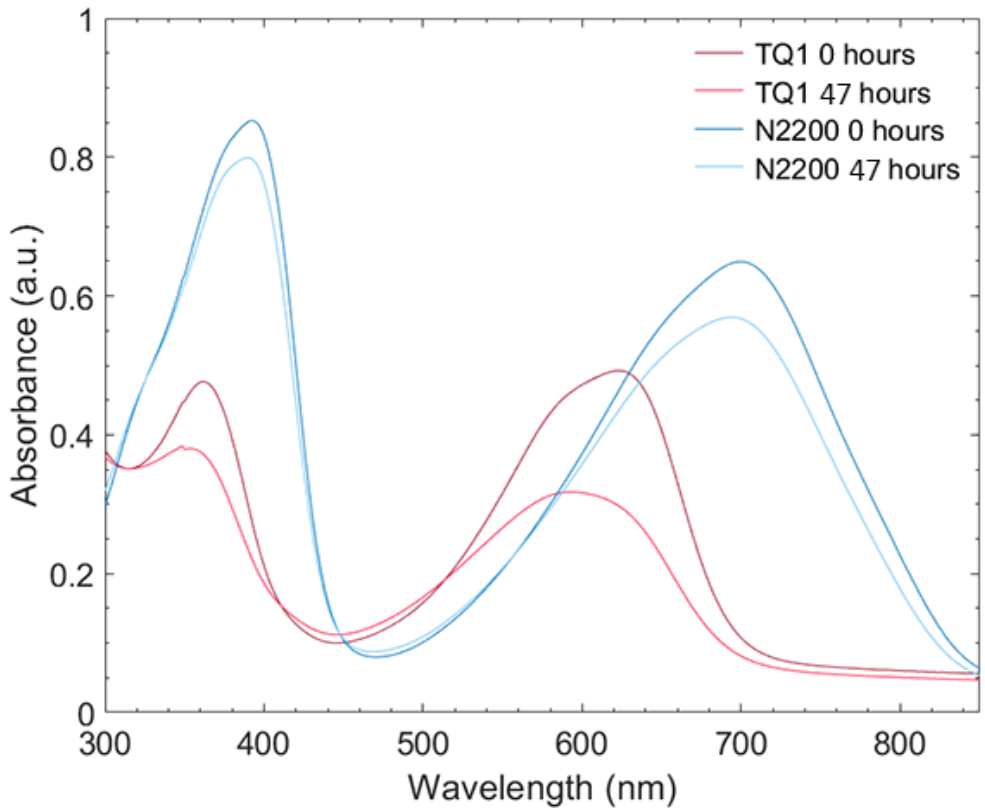

Figure 16. Absorption spectra of s*econd set of TQ1 and N2200 films, undegraded and degraded (47 hours).*

4.1.2 Solution spectra

Figure 17 shows the measured value of the absorbance of TQ1, N2200 and TQ1:N2200 blend solutions with different ratios. Figure 18 shows the calculated expected values of the blends' absorbance according to the Beer-Lambert law. The calculated values were obtained using fractions of the polymers in accordance with the volume ratio and the measured absorbance of TQ1 and N2200 (see equations (12) to (14)). By comparing the measured result with the calculated results in figure 18, one can determine that the solutions follow the linearity of the Beer-Lambert law.

$$A_{1:1} = \frac{1}{2}A_{TQ1} + \frac{1}{2}A_{N2200} \quad (12)$$

$$A_{1:2} = \frac{1}{3}A_{TQ1} + \frac{2}{3}A_{N2200} \quad (13)$$

$$A_{2:1} = \frac{2}{3}A_{TQ1} + \frac{1}{3}A_{N2200} \quad (14)$$

A_{TQ1} = absorbance of TQ1 at specific wavelength
A_{N2200} = absorbance of N2200 at specific wavelength

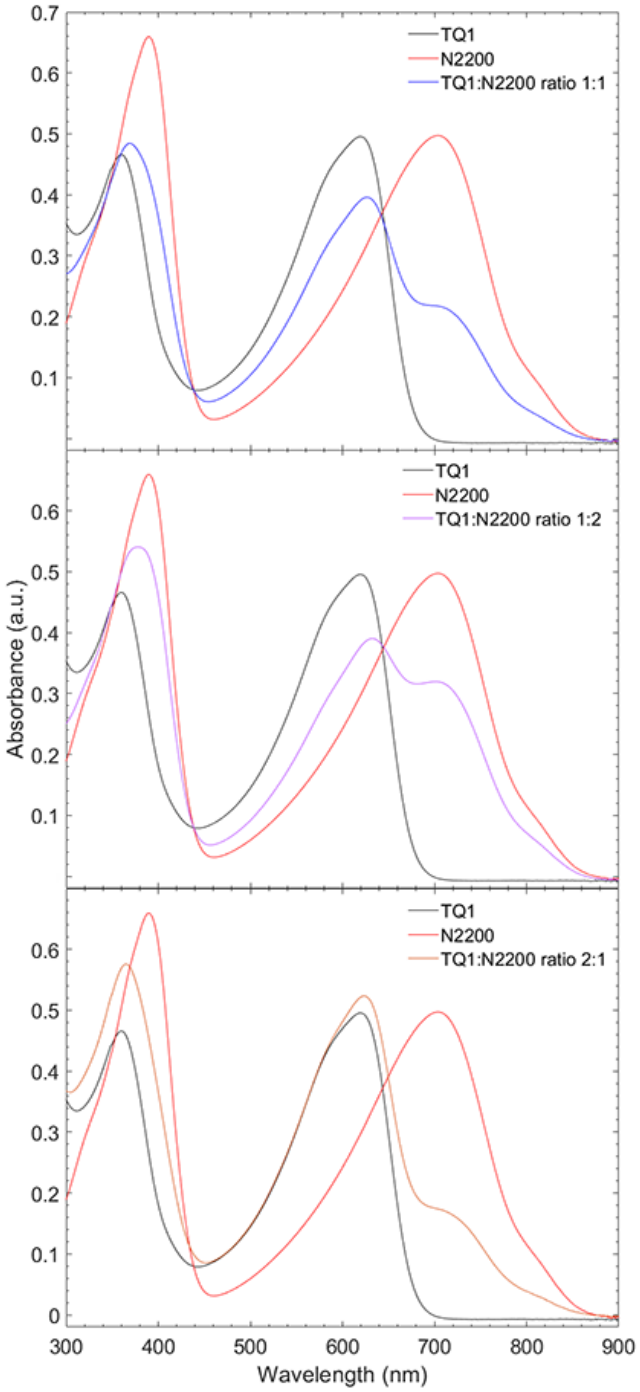

Figure 17. *Measured TQ1, N2200 and blend solution spectra.*

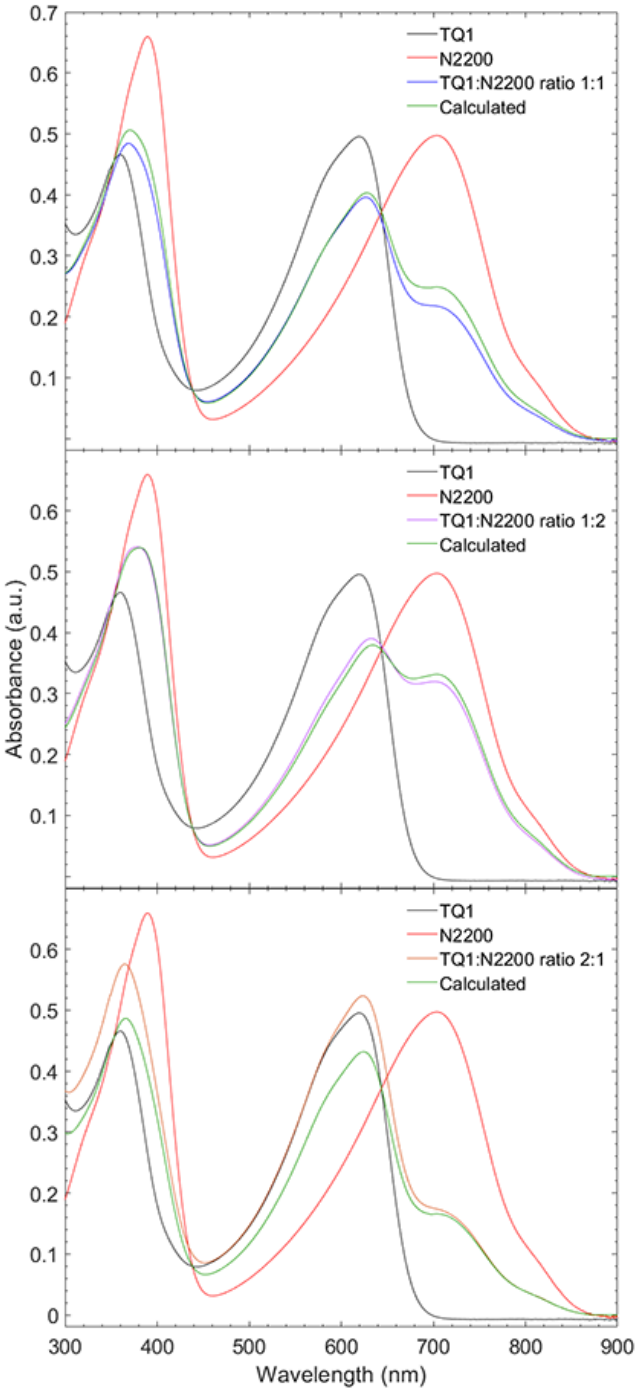

Figure 18. *Measured TQ1, N2200 and blend solution spectra, and calculated blend spectra.*

4.1.3 Comparison of solutions and thin films

The spectra of undegraded TQ1 and N2200 thin films and solutions is shown in figure 19. The peak position and full width at half maximum (FWHM) of the low energy peaks of the TQ1 and N2200 undegraded solutions, and of the TQ1 and N2200 films at different stages of degradation are shown in table 1 and 2. The FWHM for TQ1 was calculated with the base set to 0.046 a.u. This value was chosen since the absorbance saturates at 0.046 a.u. (instead of zero) when going to longer wavelength, as seen in figure 12 a). The FWHM for N2200 was measured in the spectra as they are, without any correction since the graphs do not approach any constant value when entering the IR part of the electromagnetic spectrum.

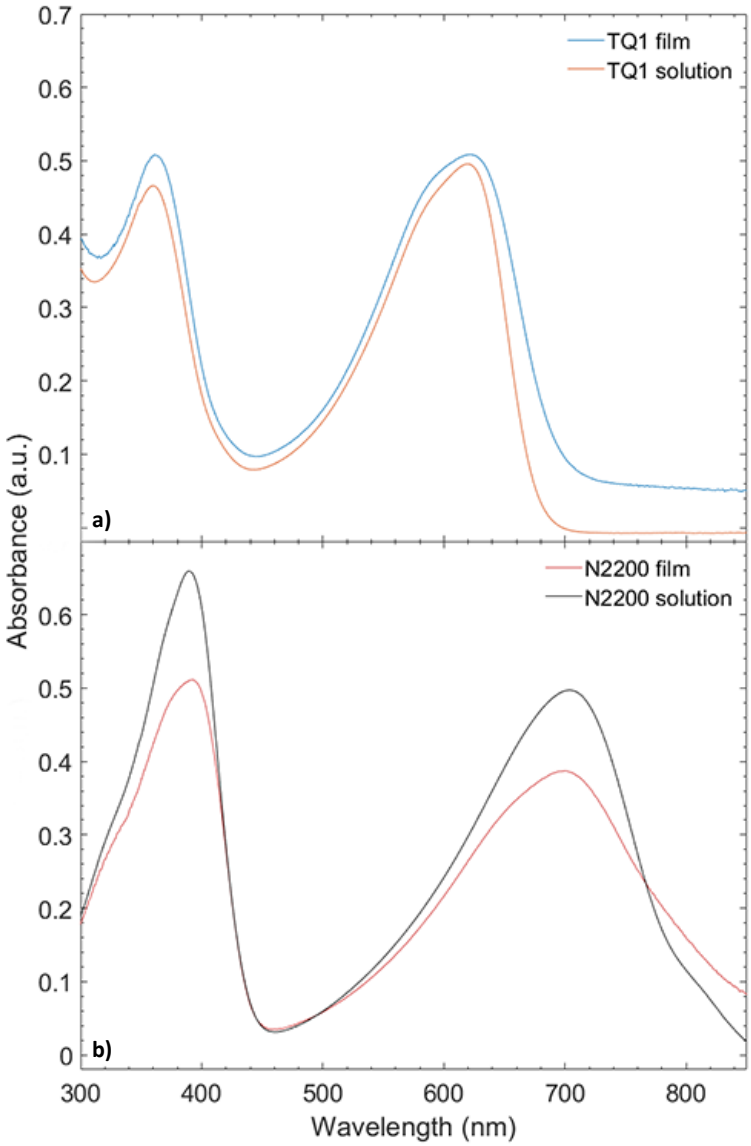

Figure 19. *TQ1 film and solution absorption spectra (a) and N2200 film and solution absorption spectra (b).*

Table 1. *FWHM and peak position of TQ1 film for different stages of degradation and undegraded TQ1 solution. (low energy peaks).*

TQ1	Solution	0h	2h	5h	10h	20h	30h	45h
Peak position (nm)	619	622	619	618	617	610	605	600
FWHM (nm)	118	128	130	132	132	135	139	143

Table 2. *FWHM and peak position of N2200 film for different stages of degradation and undegraded N2200 solution. (low energy peaks).*

N2200	Solution	0h	2h	5h	10h	20h	30h	45h
Peak position (nm)	704	700	699	698	697	696	696	695
FWHM (nm)	162	194	195	195	195	199	200	203

4.2 Atomic force microscopy

Height images of the surfaces of undegraded and degraded TQ1 and N2200 films are shown in figure 20. Figure 20 a) shows the surface of undegraded TQ1, b) shows TQ1 after 45 hours of degradation, c) shows undegraded N2200 and d) shows N2200 after 45 hours of degradation. Figure 21 a), c) and e) show the surfaces of the undegraded 1:1, 1:2 and 2:1 blend films, respectively. Figure 21 b), d) and f) show the surfaces of the 1:1, 1:2 and 2:1 blend films that were degraded for 45 hours. The N2200 film surface shows a very different morphology then the TQ1 film surface, where the N2200 film surface has a fibril-textured morphology and the TQ1 film surface has a more amorphous and bumpier morphology. All images are 2 x 2 micrometres in size.

Figures 22 a) to e) show profiles of the undegraded and degraded films and table 3 shows the Root Mean Square (RMS) roughness of the undegraded and degraded films. The profiles were measured in a horizontal direction at random locations of the images. The roughness was measured from a 1 by 1 micrometre area of each image. By studying the images, the profiles in figure 22, and the roughness values from table 3 it can be determined that the surfaces show changes before and after degradation. In the case of TQ1, several high spots that had a height of over 2 nm disappeared after degradation and the film seems to be flatter overall with lower roughness. The 1:1 and 1:2 polymer blend films also obtained a lower roughness and became flatter, while the N2200 and the 2:1 polymer blend films obtained higher roughness.

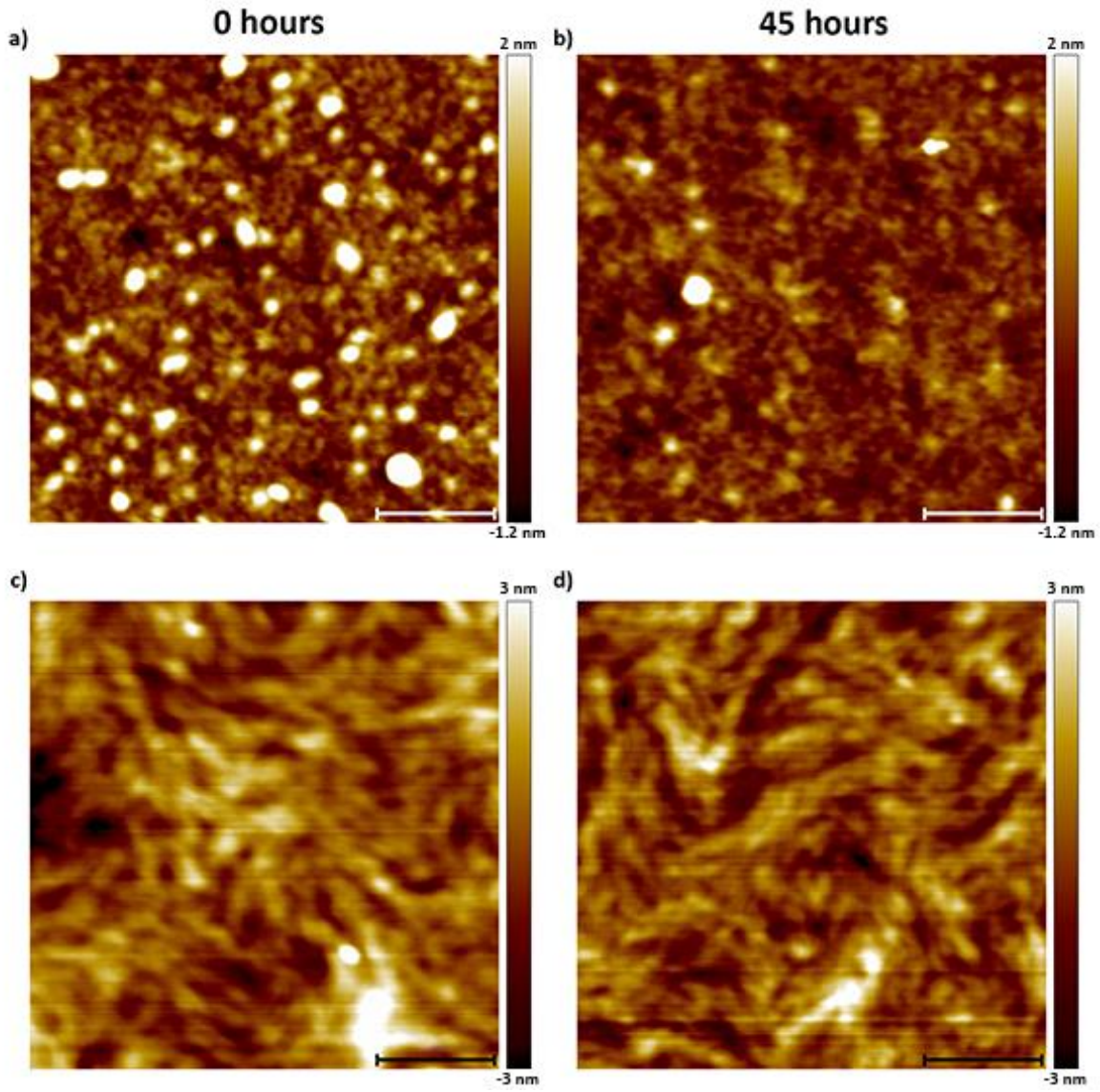

Figure 20. *AFM images of a) TQ1 film at 0 hours of degradation, b) TQ1 at 45 hours of degradation, c) N2200 at 0 hours of degradation and d) N2200 at 45 hours of degradation. The bar represents 500 nm.*

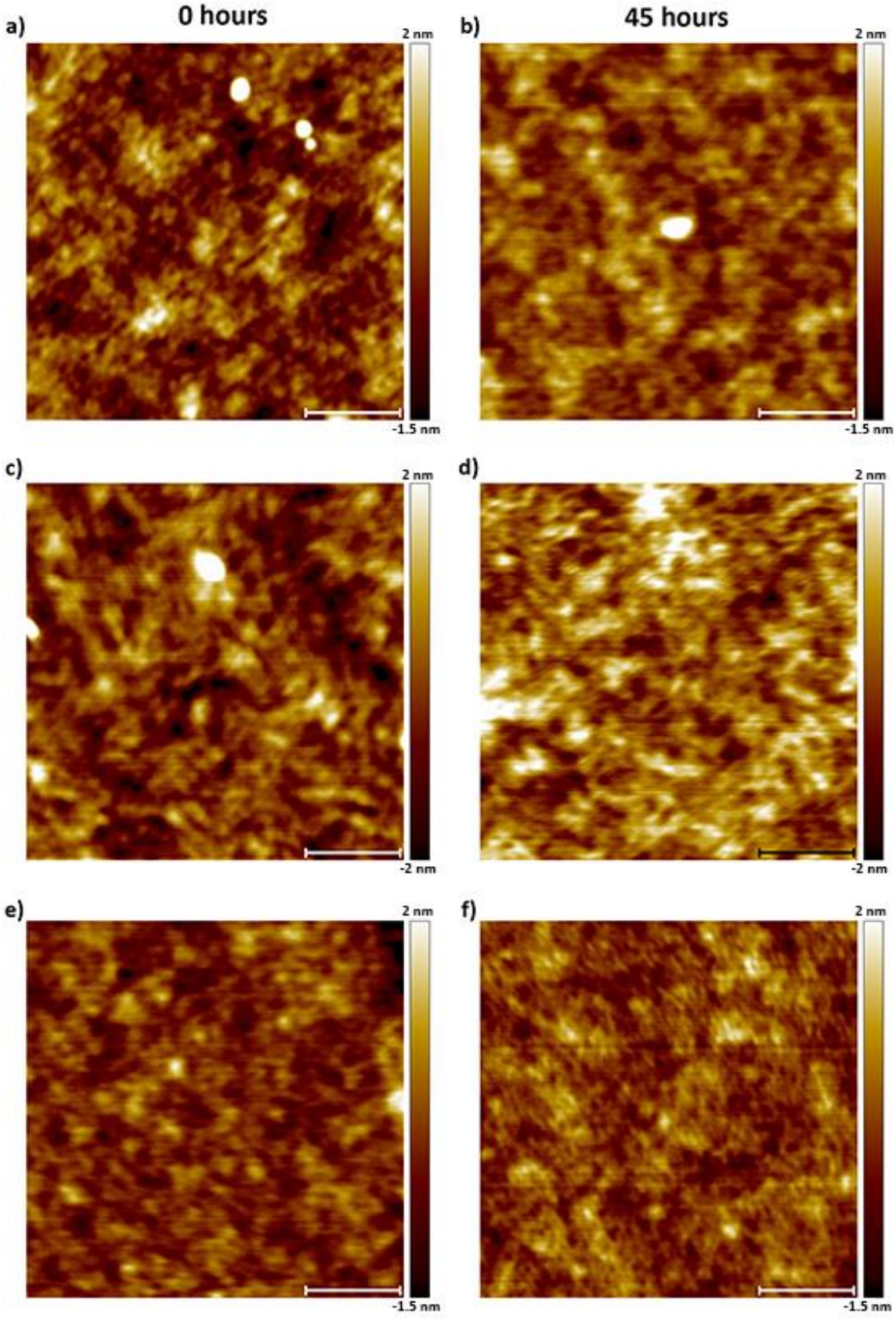

Figure 21. *AFM images of TQ1:N2200 blend films, a) shows 1:1 at 0 hours of degradation, b) 1:1 at 45 hours of degradation, c) 1:2 at 0 hours of degradation, d) 1:2 at 45 hours or degradation, e) 2:1 at 0 hours of degradation, and f) shows 2:1 at 45 hours of degradation. The bar represents 500 nm.*

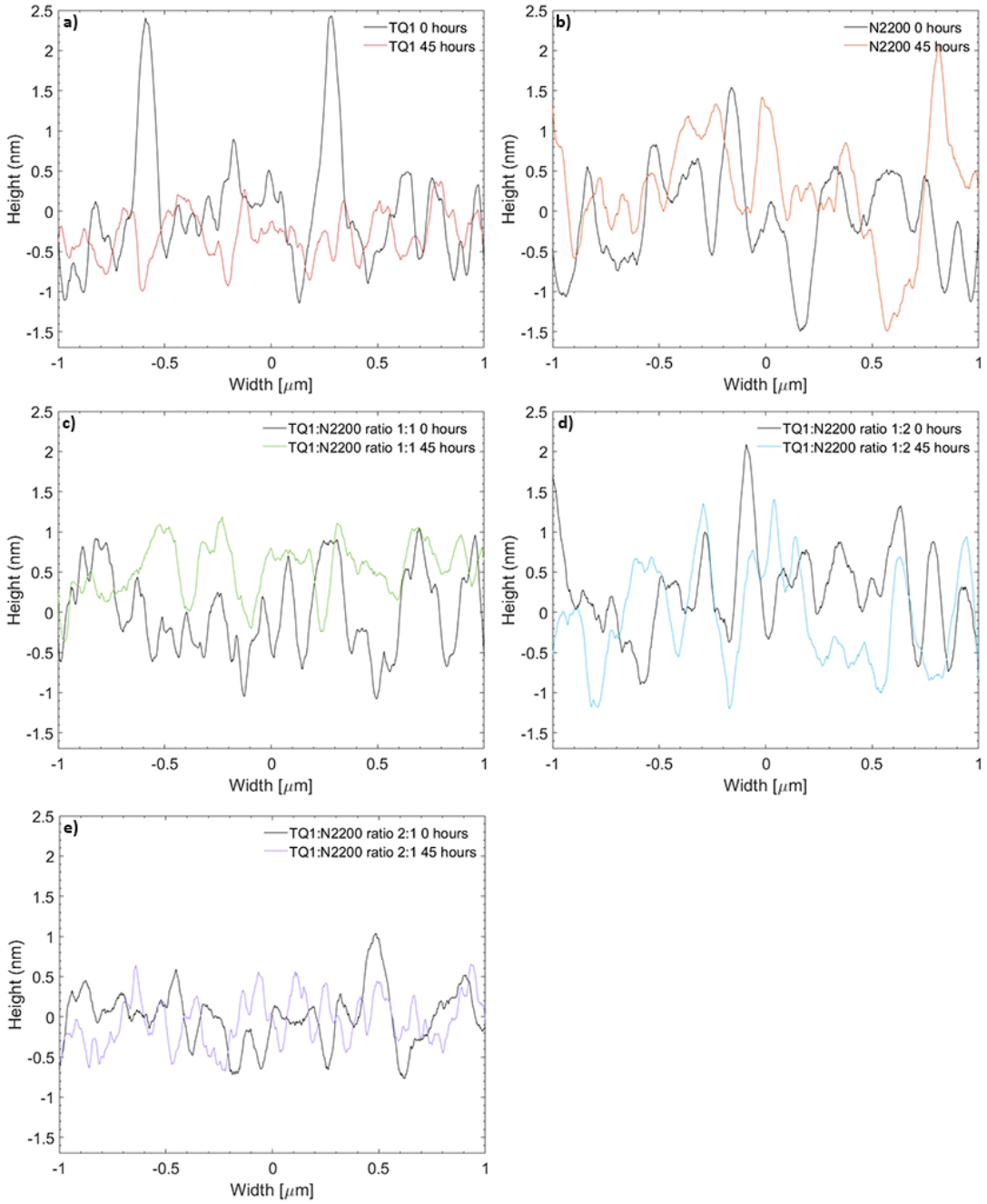

Figure 22. *Line profiles at random positions, obtained from AFM images of the film surfaces before and after 45 hours of degradation.*

Table 3. *RMS roughness, measured on a 1 x 1 micrometre area, of thin film surfaces before and after 45 hours of degradation.*

RMS roughness (pm)	TQ1	N2200	1:1	1:2	2:1
Undegraded	499	613	426	520	315
Degraded	316	670	345	467	381

5 Discussion

5.1 UV-vis spectroscopy of thin films

5.1.1 Low energy peaks

The changes observed in the UV-vis absorption spectra of thin films of the pure polymers upon exposure to simulated sunlight in air show that TQ1 films photobleach faster than N2200 films. From this we can conclude that TQ1 is more sensitive to photodegradation than N2200. This does not, however, correspond with previous work where it was found that N2200 films were more sensitive to photodegradation than TQ1 [28]. Possible reasons for this could be that the molecular weight (Mn and Mw) of the N2200 used in this work differs from that in the previous work. In this experiment the PDI for N2200 was 2.3 with a Mw of 125kg/mol, while the PDI in the previous work was 4, with a Mw of 192kg/mol. It is possible that the lower and narrower distribution of molecular weights in this work resulted in a better and more homogeneous packing of the N2200 molecules in the thin films, which in turn contributes to a lower sensitivity to photodegradation, compared with the previous work. It is however unlikely that this on its own could explain the big difference in degradation rate of N2200. Neither could this explain the difference in the degradation of TQ1 films (faster degradation in this work compared to previous work) since the same batch of TQ1 was used in both studies.

Because of this contradiction between the studies, a second set of TQ1 and N2200 films was made, and measured by absorption spectroscopy, degraded for 47 hours, and then measured again. The new result corresponds very well with the first results obtained in this study. The graphs before and after degradation are shown in figure 16 for both films. The low energy peaks of the films, which were degraded for 47 hours, lost 12.3% and 35.5% of the initial absorbance for N2200 and TQ1, respectively. Comparing these results, with the loss of 12% absorbance for N2200 and 32% absorbance for TQ1 obtained in the first measurement, show that the two results are in very good agreement. One can also see from the absorbance maxima in figure 16 that the N2200 film for the new measurement is nearly twice as thick as the N2200 film used in the first measurement. This larger film thickness closely corresponds to that used in the earlier study [28], and thus one can draw the conclusion that the thickness of the thin film does not have a large effect on the rate of photodegradation. In conclusion, while the molecular weight distribution can play a role, the complete explanation for the differences between the obtained results in this study and the ones reported in the earlier study remain currently unknown.

5.1.2 High energy peaks

How the different high energy peaks shift in the blend spectra shown in figure 13 is expected and can be explained by the shift, degradation rate and position of the pure polymer high energy peaks in figure 12. Since the N2200 contribution to the blend peaks degrades slower and is positioned at 393

nm and the TQ1 contribution degrades faster and is positioned at 360 nm, the redshift of the 1:2 blend absorption peak and the blueshift for the 2:1 blend absorption peak is expected. In the case of the 1:1 blend absorption peak, even though no shift of the peak maximum occurs, one can see a broadening of the peak towards longer wavelengths due to the strong contributions of the N2200 absorbance. As previously mentioned, the high energy peaks of TQ1 and N2200 are a result of π–π^* electron transitions. It is also worth noting that the high energy peaks follow the same pattern of degradation as the low energy peaks with regard to which film degraded faster or slower.

5.2 UV-vis spectroscopy of solutions

Following the Beer-Lambert law for absorption spectroscopy of solutions, the absorbance of the blends, given in in equations (6), should be equal to the absorbance of TQ1 and to that of N2200 for the wavelengths where TQ1 and N2200 have the same absorbance. This means that the absorbance of the pure polymer and blend solutions at these particular wavelengths should coincide. However, this is not the case, as seen in figure 17. This is most likely due to a slight deviation from the desired concentration that occurred during the dilution process. This easily happens when a volatile solvent like chloroform is used. If we correct for this deviation in concentration theoretically, calculated absorption spectra for the blends can be obtained that more correctly fit the expected outcome. Figure 23 shows the result of increasing the concentration of the blend of ratio 1:1 by 3.7% and decreasing the concentration of the blends of ratios 1:2 and 2:1 by 1.7% and 16%, respectively. As an example, the deviation of the concentration for the 2:1 blend, that resulted in an absorbance that was 16% higher than the expected absorbance, could be the result of adding 23 µl of solution instead of 20 µl in the first step of the dilution, or alternatively, that around 90 µl of solvent evaporated when the undiluted solution was kept on the magnetic stirrer heat plate, or that the amount chloroform added during the dilution was not exact. It is more likely to be a combination of these things than any single one on its own. The result of these corrections in concentration together with the calculated values for the blend spectra are seen in figure 24. It is also worth noting that concentration variations could have appeared in the diluted solutions of pure N2200 and TQ1.

The correct way of calculating the expected absorbance of the polymer blends is complicated. In this experiment it was calculated by using a factor corresponding to the volume ratio used for each polymer. However, this method does not give a perfect result. Since the polymers have weights described in two different ways, Mn, and Mw, it is unclear whether the molecular weight should be taken into account when calculating the absorbance of blends in the best way possible. Therefore, the way it was calculated in this experiment is deemed to be a good enough approximation. It would, however, be interesting to try to find a correct way to incorporate Mn and Mw when calculating the expected absorption spectra of the blend films and in that way get a more accurate result.

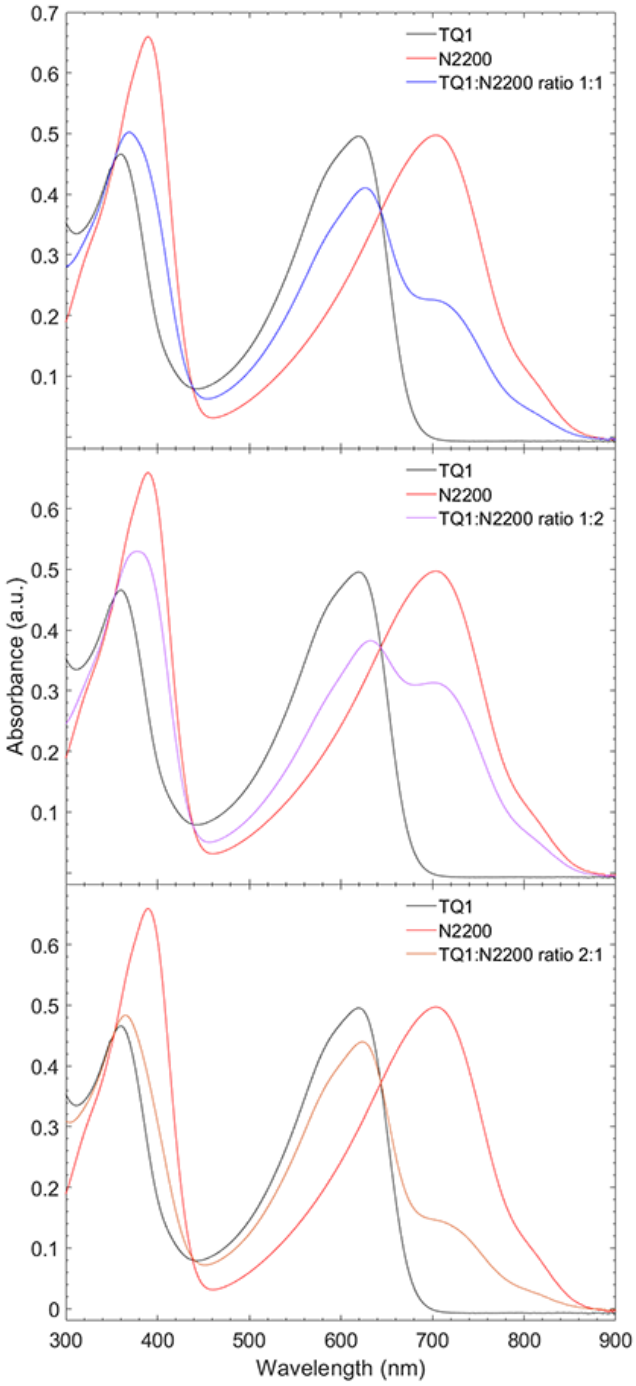

Figure 23. *TQ1, N2200 and corrected blend solution spectra*

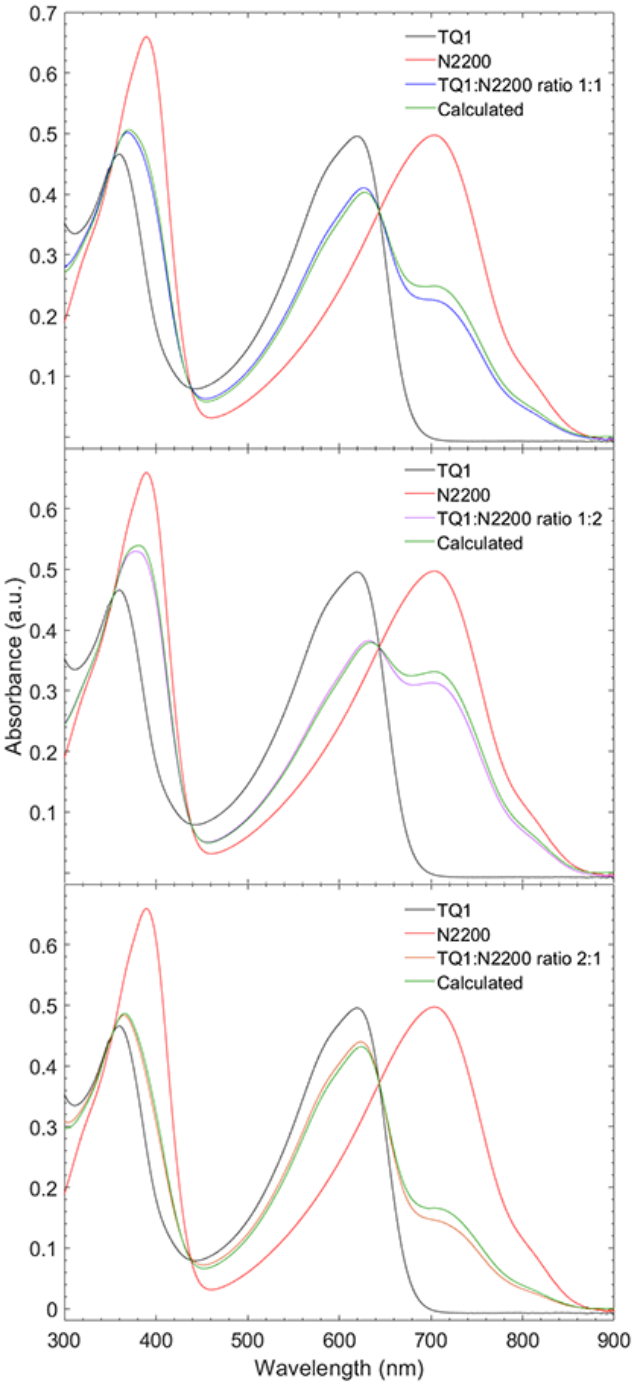

Figure 24. *TQ1, N2200 and corrected blend solution spectra with caluculated blend spectra*

5.3 Comparison of thin films and solution

The spectra of the undegraded TQ1 film and the TQ1 solution are shown in figure 19. For the TQ1 film one can see that the low energy absorption peak has two contributions, one with maximum at 622 nm and one around 590 nm. Similarly, one can see that the low energy absorption peak in the TQ1 solution spectrum has a similar shape with a contribution at 620 nm and another contribution at around 588 nm. The similarity of the solution spectrum and film spectrum of TQ1 is surprising.

The low energy absorption peak of the N2200 film also has a slight tendency to show a similar double contribution, with one maximum at around 700 nm and a shoulder at around 643 nm. The contributions to the low energy peak of the N2200 solution spectrum are less obvious, and the absorption peak appears more as one peak with a certain asymmetry.

Based on a comparison of the TQ1 spectra in figure 19 a) with the ones reported in earlier work [24] a larger difference was expected between the TQ1 solution spectrum and the TQ1 film spectrum. In this work the spectra are found to be nearly identical in shape. The TQ1 low energy peak is not as broad as expected, the reason to this remains currently unknown. However, it is worth noting that the solvent in this work differs from that of the earlier work where o-dichlorobenzene (ODCB) was used.

The FWHM values for the low energy peaks in the TQ1 and N2200 film spectra, shown in table 1, increase with increasing time of degradation. This increase of peak width could possibly be a result of several new, different transitions, from or to states that are being created due to the degradation of the molecule. However, it is hard to draw any conclusions without studying the films with other methods, such as Fourier-transform infrared spectroscopy. Furthermore, the FWHM of the low energy peak of the TQ1 solution spectrum and the undegraded TQ1 film spectrum are closer in value than expected (only 10 nm difference). One would expect the difference to be higher, as in the case of the N2200 solution and the undegraded N2200 film (32 nm difference). This broadening is expected because the number of intermolecular interactions should be much higher in a solid film than in a solution.

5.4 Atomic force microscopy

From the AFM images it is apparent that the pristine N2200 film have a different morphology than the pristine TQ1 film. The N2200 film has a fibril-textured morphology, while TQ1 has a more amorphous, bumpy surface morphology. This has also been reported in earlier works [29, 30, 31]. It has also been reported, in the case of the N2200 film, that the RMS roughness and the size of the fibrils are affected by the solvent used [31]. A fibril-texture can also be observed in the image of the N2200-rich 1:2 film, though not as clear as in the pristine N2200 film. The AFM images also showed a change in RMS roughness between the undegraded and degraded films. The change in surface structure was, however, harder do analyse with the current image quality. A higher image resolution would be needed to obtain a better understanding of the changes of the surface morphology upon exposure of the films to simulated sunlight in air. It is also important to take into consideration that the condition of the tip used for scanning plays an important role in the obtained image quality. A

sharper and cleaner tip gives a truer image of the surface. This could be a reason for a slight variation in image quality between some of the obtained images, such as the difference of the images in figure 20 a) and b). The tip was changed a couple of times during this study.

6 Conclusion

The effect of photodegradation of polymer thin films by simulated sunlight has been studied using UV-vis spectroscopy and atomic force microscopy. The polymers studied were the electron donor polymer TQ1, the electron accepting polymer N2200, and their blends of different volume ratios. The linearity of the Beer-Lambert law was also confirmed for blend solutions of the same polymers. The UV-vis spectroscopy studies have shown that N2200 is less sensitive to photodegradation than TQ1. Among the blends, the 1:2 TQ1:N2200 blend was the least sensitive to photodegradation, while the 2:1 blend was the most sensitive.

AFM imaging showed a clear change in roughness before and after degradation for thin films. TQ1 and TQ1:N2200 blends of ratio 1:1 and 1:2 obtained a lower roughness after degradation, while N2200 and the TQ1:N2200 blend of ratio 2:1 obtained a higher roughness.

6.1 Future work

To obtain more information about the degradation process of TQ1, N2200 and their blends there are several interesting measurements that can be done and parameters that can be varied such as:

- More extended studies using AFM to obtain higher quality images of the surface morphology.
- Measure the thickness of the films before and after degradation.
- Study the molecular bonds before and after degradation using Fourier-transform infrared spectroscopy to identify which chemical changes are induced by the photodegradation.
- Measure several different batches of the same polymer (with different molecular weights) to confirm the obtained results.
- Measure UV-vis spectroscopy with a DRA where the film is centre mounted and thus can measure transmittance and reflection at the same time.
- Measure the degradation of polymer solutions.
- Use other solvents for solution measurements and for coating of films.
- Study the effect of pre-annealing the film before degradation.

7 Bibliography

[1] Qishi Liu,Yufan Jiang, Ke Jin, Jianqiang Qin, Jingui Xu, Wenting Li, Ji Xiong, Jinfeng Liu, Zuo Xiao, Kuan Sun, Shangfeng Yang, Xiaotao Zhang, Liming Ding.
18% Efficiency organic solar cells.
Science Bulletin, Volume 65, Issue 4, 2020, 272-275.
doi: 10.1016/j.scib.2020.01.001

[2] Office of energy efficiency & renewable energy. Crystalline Silicon Photovoltaics Research Solar Energy Technologies Office.
Retrieval date: 2021, May 9.
https://www.energy.gov/eere/solar/crystalline-silicon-photovoltaics-research#:~:text=Crystalline%20silicon%20PV%20cells%20have,22%25%20under%20standard%20test%20conditions.

[3] Martin Green, Ewan Dunlop, Jochen Hohl-Ebinger, Masahiro Yoshita, Nikos Kopidakis, Xiaojing Hao.
Solar cell efficiency tables (version 57).
Prog Photovolt Res Appl. 2021;29:3–15.
doi: 10.1002/pip.3371

[4] Qunping Fan, a Qiaoshi An, Yuanbao Lin,c Yuxin Xia, Qian Li, Ming Zhang, Wenyan Su, Wenhong Peng, bChunfeng Zhang, Feng Liu, Lintao Hou, Weiguo Zhu, Donghong Yu, Min Xiao, Ellen Moons, Fujun Zhang, Thomas D. Anthopoulos, Olle Ingana, Ergang Wang.
Over 14% efficiency all-polymer solar cells enabled by a low bandgap polymer acceptor with low energy loss and efficient charge separation.
Energy Environ. Sci., 2020, 13, 5017.
doi: 10.1039/d0ee01828g

[5] Wenchao Huang, Eliot Gann, Naresh Chandrasekaran, Shyamal K. K. Prasad, Sheng-Yung Chang, Lars Thomsen, Dinesh Kabra, Justin M. Hodgkiss, Yi-Bing Cheng,Yang Yang, and Christopher R. McNeill.
Influence of Fullerene Acceptor on the Performance, Microstructure, and Photophysics of Low Bandgap Polymer Solar Cells.
Adv. Energy Mater. 2017, 7, 1602197.
doi: 10.1002/aenm.201602197

[6] Havid Aqoma, Sujung Park, Hye-Yun Park, Wisnu Tantyo Hadmojo, Seung-Hwan Oh, Sungho Nho, Do Hui Kim, Jeonghoon Seo, Sungmin Park, Du Yeol Ryu, Shinuk Cho, and Sung-Yeon Jang.
11% Organic Photovoltaic Devices Based on PTB7-Th: PC71BM Photoactive Layers and Irradiation-Assisted ZnO Electron Transport Layers.
Adv. Sci. 2018, 5, 1700858.
doi: 10.1002/advs.201700858

[7] Andreas Distler, Tobias Sauermann, Hans-Joachim Egelhaaf, Sheila Rodman, Waller, Kap-Soo Cheon, Mike Lee, and Dirk M. Guldi.
The Effect of PCBM Dimerization on the Performance of Bulk Heterojunction Solar Cells.
Adv. Energy Mater. 2014, 4, 1300693.
doi: 10.1002/aenm.201300693

[8] Fortunato Piersimoni, Giedrius Degutis, Sabine Bertho, Koen Vandewal, Donato Spoltore, Tim Vangerven, Jeroen Drijkoningen, Marlies K. Van Bael, An Hardy, Jan D'Haen, Wouter Maes, Dirk Vanderzande, Milos Nesladek, Jean Manca.
Influence of fullerene photodimerization on the PCBM crystallization in polymer: Fullerene bulk heterojunctions under thermal stress.
Journal of Polymer Science Part B: Polymer Physics Volume: 51 Issue 16 (2013).
doi: 10.1002/polb.23330

[9] Ana S.Anselmo, Andrzej Dzwilewski, Krister Svensson, Ellen Moons.
Photodegradation of the electronic structure of PCBM and C60 films in air.
Chemical Physics Letters, Volume 652, 2016, Pages 220-224.
doi: 10.1016/j.cplett.2016.04.003

[10] Rickard Hansson, Camilla Lindqvist, Leif K. E. Ericsson, Andreas Opitz, Ergang Wang and Ellen Moons.
Photo-degradation in air of the active layer components in a thiophene-quinoxaline copolymer:fullerene solar cell.
Phys. Chem. Chem. Phys. 2016, 18, 11132.
doi: 10.1039/c5cp07752d

[11] He Yan1, Zhihua Chen, Yan Zheng, Christopher Newman, Jordan R. Quinn, Florian Dötz, Marcel Kastler & Antonio Facchetti.
A high-mobility electron-transporting polymer for printed transistors.
Nature 457, 679–686 (2009).
doi: 10.1038/nature07727

[12] Lei Zhu, Wenkai Zhong, Chaoqun Qiu, Bosai Lyu, Zichun Zhou, Ming Zhang, Jingnan Song, Jinqiu Xu, Jing Wang, Jazib Ali, Wei Feng, Zhiwen Shi, Xiaodan Gu, Lei Ying, Yongming Zhang, Feng Liu
Aggregation-Induced Multilength Scaled Morphology Enabling 11.76% Efficiency in All-Polymer Solar Cells Using Printing Fabrication.
Adv. Mater. 2019, 31, 1902899
doi: 10.1002/adma.201902899

[13] Yiho Kim, Hye Rim Yeom, Jin Young Kim and Changduk Yang.
High-efficiency polymer solar cells with a cost-effective quinoxaline polymer through nanoscale morphology control induced by practical processing additives.
Energy Environ. Sci., 2013, 6, 1909.
doi: 10.1039/c3ee00110e

[14] David I. Bower (2002). An introduction to polymer physics. 1st Ed. Cambridge University Press.

[15] Polymer Molecular Weight Distribution and Definitions of Mw Averages, Agilent Technologies. (2015, April 30). Retrieval date: 2021, April 5. https://lcms.cz/labrulez-bucket-strapi-h3hsga3/5990_7890_EN_990bf6319d/5990-7890EN.pdf

[16] JordiLabs. Mw Averages Explanations. (2017, Feb.). Retrieval date: 2021, April 5. https://jordilabs.com/wp-content/uploads/2017/02/White-Paper-Mw-Averages-Explanation.pdf

[17] Caltech. Diffuse Reflectance Accessory (external) Manual for the Cary 4000, 5000 and 6000i. Retrieval date: 2021, April 5. https://mmrc.caltech.edu/Cary%20UV-Vis%20Int.Sphere/manuals/Cary%20manuals/4000_5000_6000i_external_dra.pdf

[18] Jeffrey L. Taylor. Integrating Sphere Functionality: The Scatter Transmission Measurement. (2015, April 30). Retrieval date: 2021, April 5. https://www.perkinelmer.com/cmsresources/images/44-156124tch_011486_01_integratingspherefunctionalitythescattertransmissionmeasurement.pdf

[19] Agilent Technologies. Fundamentals of UV-vis spectroscopy. Primer. (2015, July 23) Retrieval date: 2021, April 5. https://www.agilent.com/cs/library/primers/public/59801397_020660.pdf

[20] F. James Holler, Douglas A. Skoog, Stanley R. Crouch. (2007). Principles of instrumental analysis. 6th ed. Thomson Brooks/Cole.

[21] Svante Hedström and Petter Persson. Quantum Chemical Calculations of Side-Group Stacking and Electronic Properties in Thiophene−Quinoxaline Polymers. J. Phys. Chem. C 2012, 116, 26700−26706. doi: 10.1021/jp308063u

[22] Sebastian T. Hoffmann, Heinz Bässler, and Anna Köhler. What Determines Inhomogeneous Broadening of Electronic Transitions in Conjugated Polymers? J. Phys. Chem. B 2010, 114, 17037–17048. doi: 10.1021/jp107357y

[23] Craig B. Fryhle, Scott A. Snyder, T. W. Graham Solomons. (2016). Solomons's organic chemistry. 12th ed. John Wiley & Sons.

[24] Ergang Wang, Lintao Hou, Zhongqiang Wang, Stefan Hellström, Fengling Zhang, Olle Inganäs, Mats R. Andersson.
An Easily Synthesized Blue Polymer for High-Performance Polymer Solar Cells.
Advanced Materials. 22(46):5240-5244.
doi: 10.1002/adma.201002225

[25] Hao Zhang, Yongzhen Wu, Weiwei Zhang, Erpeng Li, Chao Shen, Huiyun Jiang, He Tian and Wei-Hong Zhu.
Low cost and stable quinoxaline-based holetransporting materials with a D–A–D molecular configuration for efficient perovskite solar cells.
Chem. Sci., 2018, 9, 5919.
doi: 10.1039/c8sc00731d

[26] Ranbir Singh, Georgia Pagona, Vasilis G. Gregoriou, Nikos Tagmatarchis, Dimosthenis Toliopoulos, Yang Han, Zhuping Fei, Athanasios Katsouras, Apostolos Avgeropoulos, Thomas D. Anthopoulos, Martin Heeney, Panagiotis E. Keivanidis and Christos L. Chochos
The impact of thienothiophene isomeric structures on the optoelectronic properties and photovoltaic performance in quinoxaline based donor– acceptor copolymers.
Polym. Chem., 2015, 6, 3098.
doi: 10.1039/c5py00075k

[27] Robert Steyrleuthner, Marcel Schubert, Ian Howard, Bastian Klaumü nzer, Kristian Schilling, Zhihua Chen, Peter Saalfrank, Fredé ric Laquai, Antonio Facchetti, and Dieter Neher.
Aggregation in a High-Mobility n-Type Low-Bandgap Copolymer with Implications on Semicrystalline Morphology.
Chem. Soc. 134 (2012) 18303-18317.
doi: 10.1021/ja306844f

[28] Vanja Blazinic. (2019).
Probing the effects of photodegradation of acceptor materials in polymer solar cells: bulk, surface, and molecular level [Doctoral thesis] Karlstad University.
Paper V. Stability of TQ1:N2200 active layers for all-polymer solar cells.
Vanja Blazinic, Leif Ericsson K. E. Ericsson, Ellen Moons.

[29] Yuxin Xia, Chiara Musumeci, Jonas Bergqvist, Wei Ma, Feng Gao, Zheng Tang, Sai Bai, Yizheng Jin, Chenhui Zhu, Renee Kroon, Cheng Wang, Mats R. Andersson, Lintao Hou, Olle Inganas, Ergang Wang.
Inverted all-polymer solar cells based on a quinoxaline–thiophene/naphthalene-diimide polymer blend improved by annealing.
J. Mater. Chem. A, 2016, 4, 3835.
doi: 10.1039/c6ta00531d

[30] Jian Liu, Li Qiu, Riccardo Alessandri, Xinkai Qiu, Giuseppe Portale, JingJin Dong, Wytse Talsma, Gang Ye, Aprizal Akbar Sengrian, Paulo C. T. Souza, Maria Antonietta Loi, Ryan C. Chiechi, Siewert J. Marrink, Jan C. Hummele, L. Jan Anton Koster.
Enhancing Molecular n-Type Doping of Donor-Acceptor Copolymers by Tailoring Side Chains.
Advanced Materials, 30(7), 1704630.
doi:10.1002/adma.201704630

[31] Alessandro Luzio, Luigino Criante, Valerio D'Innocenzo, Mario Caironi.
Control of charge transport in a semiconducting copolymer by solvent-induced long-range order.
Sci Rep 3, 3425 (2013).
doi: 10.1038/srep03425